Dynamic regulation of CD28 conformation and signaling by charged lipids and ions

Wei Yang[1, 2, 7], Weiling Pan[1, 7], Shuokai Chen[1, 7], Nicola Trendel[3, 7], Shutan Jiang[1, 7], Feng Xiao[4], Manman Xue[1], Wei Wu[1], Zeli Peng[1], Xiaoxi Li[5], Hongbin Ji[5], Xiaolong Liu[5], Hai Jiang[5], Haopeng Wang[6], Hongbin Shen[4], Omer Dushek[3, 8], Hua Li[1, 8], Chenqi Xu[1, 6, 8]

[1]State Key Laboratory of Molecular Biology, National Center for Protein Science Shanghai, Shanghai Science Research Center, CAS Center for Excellence in Molecular Cell Science, Shanghai Institute of Biochemistry and Cell Biology, Chinese Academy of Sciences; University of Chinese Academy of Sciences, 320 Yueyang Road, Shanghai 200031, China.

[2]Department of Pathology, School of Basic Medical Sciences, Southern Medical University, Guangzhou 510515, China

[3]Sir William Dunn School of Pathology, University of Oxford, South Parks Road, Oxford, Oxfordshire OX1 3RE, UK

[4]Institute of Image Processing & Pattern Recognition, Shanghai Jiaotong University, Shanghai 200240, China

[5]State Key Laboratory of Cell Biology, CAS Center for Excellence in Molecular Cell Science, Institute of Biochemistry and Cell Biology, Shanghai Institutes for Biological Sciences, Chinese Academy of Sciences, University of Chinese Academy of Sciences, Shanghai 200031, China;

[6]School of Life Science and Technology, ShanghaiTech University, Shanghai 201210, China

[7]These authors contribute equally to the paper

[8]Correspondence to Chenqi Xu (cqxu@sibcb.ac.cn), Hua Li (lihua@sibcb.ac.cn), Omer Dushek (omer.dushek@path.ox.ac.uk)

Abstract

CD28 provides an essential co-stimulatory signal for T cell activation and its function is critical in antitumor immunity. However, the molecular mechanism of CD28 transmembrane signaling remains elusive. Here, we find that CD28 conformation and signaling are regulated by two counteractive charged factors, i.e. acidic phospholipid and Ca^{2+} ion. NMR structure shows that acidic phospholipids can sequester CD28 signaling motifs within the membrane, thus limiting CD28 basal signaling. T-cell receptor (TCR) activation induces local [Ca^{2+}] increase around CD28, and Ca^{2+} can use its charges to directly disrupt CD28-lipid interaction, which leads to CD28 opening and signaling. TCR, Ca^{2+}, and CD28 together form a dual positive feedback circuit to significantly amplify T cell signaling and therefore increase antigen sensitivity. This work unravels a new regulatory mechanism of CD28 signaling, contributing to the understanding of the dependence of the co-stimulation signaling on TCR signaling and the high sensitivity of T cells.

INTRODUCTION

T cells are central players in immune responses to exogenous pathogens and endogenous cancers. T cell activation requires two signals: a major antigen-induced signal from the T cell receptor (TCR) and a secondary signal from co-stimulatory receptors[1,2]. The most well studied co-stimulatory receptor is CD28, which has a crucial function in T cell activation. Without CD28 signaling, TCR signaling alone induces T cells to enter an anergic state where they lose responsiveness to further antigen stimulation[3,4]. Signaling from CD28 can increase T cell sensitivity, cytokine production, and cell survival. Also, CD28 signaling regulates T cell development, differentiation, and trafficking[5-11]. The important roles of CD28 in regulating T cell activation have been exploited therapeutically. For example, CTLA4-Ig, a high affinity competitor of CD28 for ligand binding, has been used clinically to treat rheumatoid arthritis and to extend graft survival in kidney transplantation[12,13]. The signaling domain of CD28 is also routinely incorporated into Chimeric Antigen Receptor (CAR) therapies to treat hematological cancers[14]. More recently, CD28 function has been found to be crucial in anti-PD-1 caner immunotherapy[15,16].

Signaling from CD28 relies on the conserved 41-a.a. cytoplasmic domain, which has multiple signaling motifs but lacks catalytic activity[17]. The YxxM and PYAP are dominant motifs localized at the N and C-terminal regions[1,3,4,18]. The YxxM motif recruits the p85 subunit of PI3K, Grb2 and GADS through pTyr-dependent interaction with SH2 domain. The PYAP motif interacts with signaling proteins, such as Lck and Grb2, through phosphorylation-independent interaction with SH3 domain. The phosphorylated PYAP motif can interact with Lck SH2 domain and in turn recruit PKCθ[19]. These molecular interactions eventually lead to the activations of key transcription factors NFAT1, NFκB and AP-1 to regulate T cell activation and function. Besides the YxxM and PYAP motifs, the highly conserved polybasic region is required for Lck recruitment[20].

Despite extensive studies, several key questions concerning CD28 signaling remain unanswered. First, how is CD28 activity restrained in resting T cells? If the cytoplasmic domain of CD28 was freely exposed in the cytosol, it would be difficult to avoid phosphorylation-independent interactions with downstream signaling molecules. Second, why is CD28 signaling dependent on TCR signaling? Engagement of CD28 with its native ligands (CD80 and CD86), in the absence of ligands to the TCR, leads to transient transcription of only a few genes and does not lead to T cell activation[21,22]. However, in the presence of TCR ligands, CD28 can significantly augment TCR signaling to fully activate T cells. The molecular mechanism underlying this signaling hierarchy is incompletely understood. Third, how does CD28 signaling contribute to the high sensitivity of T cells to antigen?

In this work, we find that CD28 activity is regulated by negatively-charged acidic phospholipids and positively-charged Ca^{2+} ions. Acidic phospholipids sequester CD28 signaling motifs within the membrane via ionic CD28-lipid interaction, which provides a safety control on CD28 activity in resting T cells. TCR-induced Ca^{2+} influx removes the safety control and leads to CD28 opening and signaling, which explains the dependence of CD28 signaling on TCR signaling. We formulate a mathematical model that is consistent with our experimental observations and find that the underlying positive feedback circuit among TCR, Ca^{2+} and CD28 provides a signaling basis for the high sensitivity of T cells to antigens. This work thus reports a new regulatory mechanism for CD28 signaling that addresses several key questions of co-stimulation in T cell activation.

RESULTS

CD28 contains conserved juxtamembrane polybasic regions to bind with acidic phospholipids

Previous studies have shown that negatively-charged acidic phospholipids can ionically interact with positively-charged juxtamembrane polybasic regions (PBRs) of membrane proteins to regulate protein structure and function[23], such as the case for T cell receptor[24-31]. To address whether ionic protein-lipid regulation has a general application, we performed a systematic bioinformatics analysis to analyze the isoelectric point (pI) values of the first 10 amino acid sequences in the cytoplasmic domains of single-pass membrane proteins that localizes at the plasma membrane (**Supplementary Fig. 1**). Most proteins show pI values higher than 7 and more than 40% of them are higher than 11. There is no clear difference between membrane proteins in immune and total cells. Many important membrane proteins in immune cells, such as CD28, Notch1 (also named NOTC1), and PD1L1, contain juxtamembrane PBRs (**Supplementary Data Set 1**). Given the functional importance of CD28, we studied its lipid regulation in the following.

Analysis of CD28 cytoplasmic domain ($CD28_{CD}$) from different species showed that the basic residues are highly conserved (**Supplementary Figs. 2a, b**). An equilibrium-based microdialysis assay was performed to assess the binding of $CD28_{CD}$ WT and mutants with different lipid species (**Supplementary Figs. 2c, d**). $CD28_{CD}$ specifically interacted with acidic phospholipids but not with zwitterionic phospholipids (**Supplementary Fig. 2e**). However, $CD28_{CD}$ did not show a strong preference to a particular acidic phospholipid, which is a typical feature of ionic protein-lipid interaction[23]. Mutating the basic residues in either of the two PBRs nearly abolished the lipid binding of $CD28_{CD}$ (CD28_M1 and CD28_M2), whereas

mutating the basic residues at the C-terminal region had relatively minor effect (CD28_M3) (**Supplementary Figs. 2f,g**). We further used a biophysical method, Aromatic Fluorescence Emission (AFE) assay, to measure the intrinsic fluorescence emission of $CD28_{CD}$ aromatic residues (**Supplementary Fig. 3**). Incubation with acidic phospholipid vesicles but not zwitterionic phospholipid vesicles led to significant increase of AFE value of $CD28_{CD}$, suggesting that membrane binding changed the local environment of functional tyrosines. Consistent with our data, live-cell FRET experiment shows that $CD28_{CD}$ has PBR-dependent binding to the plasma membrane in T cells[20]. It is therefore evident that $CD28_{CD}$ PBRs can specifically bind to acidic phospholipids via ionic interactions.

To further support that our bioinformatic analysis of potential lipid-binding sequence is valid, we investigated another molecule Notch1. The juxtamembrane polybasic region of Notch1 showed clear binding to acidic phospholipids in the AFE assay. A live-cell FRET strategy[25] was also used to study Notch1-membrane binding in T cells. We attached the Notch1 juxtamembrane polybasic region (first 20aa sequence in the cytoplasmic domain) with a C-terminal mTFP to the TM domain of an irrelevant monomeric membrane protein KIR2DL3. The KIR-Notch1-mTFP chimera was stably expressed in Jurkat cells and the de-quenching FRET was performed to measure the FRET efficiency between Notch1-mTFP and membrane-labeling dye R18. 3aa-mTFP and 25aa-mTFP, that have flexible linkers with different lengths between the transmembrane domain and the mTFP moiety, were used as controls to mimic the FRET level of membrane-bound or membrane-dissociated Notch1. The FRET experiment showed the Notch1 juxtamembrane region can indeed bind to the plasma membrane in live T cells (**Supplementary Fig. 4**).

Membrane insertion of the $CD28_{CD}$ signaling motifs

We next used solution NMR to study $CD28_{CD}$-lipid interaction at atomic resolution. The two-dimensional ^{1}H-^{15}N transverse relaxation optimized spectroscopy (TROSY) of $CD28_{CD}$ in solution showed features of a flexible peptide with limited dispersion of amide resonances (**Fig. 1a**). We next prepared lipid bicelles with different charge properties to study binding of $CD28_{CD}$ with different phospholipid species. Adding zwitterionic POPC bicelles (q=0.8) to $CD28_{CD}$ did not induce a detectable resonance shift, which confirmed that $CD28_{CD}$ did not bind to zwitterionic phospholipids. In contrast, adding acidic POPG bicelles (q=0.8) induced significant shifts on nearly every amide resonance peak (**Fig. 1a**), which confirmed that $CD28_{CD}$ specifically bound to acidic phospholipid.

We next investigated this interaction in more detail with additional NMR methods. In the context of POPG bicelles, all the $CD28_{CD}$ residues were assigned with the exception of two N-terminal residues that were in fast exchange with water and the proline residues that lack backbone amide protons (**Fig. 1b**). In order to study the position of $CD28_{CD}$ relative to the lipid bilayer, we measured intermolecular (i.e.

protein-to-lipid) Nuclear Overhauser Effects (NOEs) to obtain distance information. We first measured intermolecular NOEs between peptide backbone amide protons and lipid protons (**Fig. 1c**). The NOEs were categorized into three groups: NOEs between $CD28_{CD}$ backbone amide protons and lipid acyl chain protons, lipid headgroup protons, and water protons (**Fig. 1d**). Notably, the lipid headgroup region is hydrated with water molecules with high concentration. Most $CD28_{CD}$ backbone amide protons displayed NOEs to both lipid acyl chains and water molecules, suggesting that $CD28_{CD}$ backbone resided at the interface between hydrophobic lipid acyl chain region and hydrophilic headgroup region. Compared with residues in the C-terminal region including the PYAP motif, the residues in the N-terminal region including the YxxM motif displayed more NOEs with acyl chains, suggesting a deeper insertion of the N-terminal region into the hydrophobic membrane interior.

We next measured NOEs between methyl and aromatic sidechains of $CD28_{CD}$ with lipids (**Figs. 1e-f**). Almost all methyl protons from Leu and Met showed strong NOEs to lipid acyl chains but not lipid headgroups (**Fig. 1e**). These data indicated that the aliphatic sidechains of $CD28_{CD}$ were deeply inserted into the membrane hydrophobic core. The aromatic protons of tyrosines also showed strong NOEs to lipid acyl chains. However, only one set of intermolecular NOEs from tyrosine Hδ and Hε protons were detected, indicating that the NOE signals from the four tyrosines (Tyr14, Tyr29, Tyr32, and Tyr41) were heavily overlapped (**Fig. 1f**). In order to determine the contribution of the key tyrosines in the YxxM (Tyr14) and the PYAP (Tyr32) motifs to lipid interactions, we generated mutants where all tyrosines were mutated to phenyalanines with the exception of either Tyr14 (CD28_M4) or Tyr32 (CD28_M5) (**Fig. 1g**). The aromatic protons of Tyr14 and Tyr32 all showed NOEs to lipid acyl chains (**Fig. 1f**). Furthermore, the NOEs from Tyr14 were stronger than those from Tyr32, indicating that both Tyr14 and Tyr32 were inserted into the membrane hydrophobic core but with different insertion depths. Therefore, most of the hydrophobic residues, particularly the functionally important YxxM and PYAP motifs, were deeply inserted into the hydrophobic interior of the membrane bilayer.

NMR structure and dynamics of membrane-bound $CD28_{CD}$

We next determined the structure of membrane-bound CD28 in the context of a lipid bilayer using Xplor-NIH[32]. Two sets of NOE restraints were utilized in the structure calculation: protein intramolecular NOE restraints measured by the ^{15}N- and ^{13}C-separated NOESY (NOE spectroscopy) experiments and protein-lipid intermolecular NOEs measured by the protein-lipid NOESY experiments. In the Xplor-NIH program, an atom-to-plane potential was introduced to convert intermolecular distance restraints to positional information of protein atoms within lipid planes[25]. To this end, three parallel planes representing different parts of the membrane bilayer were set: the 1st lipid headgroup glycerol plane, the 2nd lipid headgroup glycerol plane, and the lipid acyl chain plane. Then the protein-lipid NOEs

were used to position $CD28_{CD}$ atoms at different planes. As a result, an ensemble of 200 structures was calculated from 192 protein NOE-derived restraints and 119 plane restraints (**Table 1**). Overall, the $CD28_{CD}$ backbone was mainly localized at the interface between the hydrophilic headgroup region and the hydrophobic core of the membrane (**Figs. 2a-c**). This position of $CD28_{CD}$ can facilitate ionic interactions of basic residue sidechains with phosphate groups in lipid headgroups as well as insertions of hydrophobic residue sidechains into the membrane hydrophobic interior. Furthermore, there was a tendency that the N-terminus was inserted deeper into the lipid bilayer than the C-terminus. The key tyrosines in both the YxxM and PYAP motifs were inserted into the membrane hydrophobic core (**Figs. 2a, d-e**), which would render them inaccessible to cytosolic tyrosine kinases. Furthermore, the basic residues in PBRs were orientated toward the membrane headgroups, thus facilitating their ionic interactions (**Figs. 2f-g**).

Close inspection of $CD28_{CD}$ intramolecular NOE restraints showed that there were no NOEs characteristic of secondary structures and no medium- or long-range NOEs. Therefore, the conformation of the membrane-bound $CD28_{CD}$ was largely dynamic. We further performed the backbone amide ^{15}N spin relaxation experiment to study the intrinsic dynamics of membrane-bound $CD28_{CD}$ at fast timescale (ps-ns). The ^{15}N relaxation parameters of the $CD28_{CD}$ backbone signals, including R1, R2 and the heteronuclear ^{1}H-^{15}N NOE, were determined (**Supplementary Fig. 5**). The ^{1}H-^{15}N NOE values showed variations ranged from 0.07 to 0.69 with an average of 0.46. In general, flexible residues give ^{1}H-^{15}N NOE values less than 0.65. Therefore, the lipid-bound $CD28_{CD}$ should be very flexible. R1 values of the $CD28_{CD}$ residues were larger compared with globular and stably folded proteins and showed relatively small variation (0.89 ~ 1.84 s^{-1}), with an average value of 1.28 s^{-1}. Large R1 values imply large internal motion that is independent of conformational exchange. R2 values of $CD28_{CD}$ residues were small, also indicating fast internal motion. In contrast to R1 values, R2 values showed a larger variation (11.12 ~ 66.76 s^{-1}), with an average value of 26.81 s^{-1}. The C-terminus of $CD28_{CD}$ had smaller R2 and ^{1}H-^{15}N NOE values than other regions, suggesting that this part might be more dynamic. These data together supported the conclusion that the lipid-bound $CD28_{CD}$ remained dynamic even when fully embedded in the membrane bilayer.

Association of $CD28_{CD}$ with the membrane regulates the basal signaling of CD28

To further study the role of membrane association of $CD28_{CD}$ in the co-stimulatory function of CD28, we designed a CD28 mutant with impaired membrane binding property. We first attempted to use the M1 and M2 mutants but found that they had a defect in Lck recruitment and lower levels of phosphorylation, which is consistent with a previous report[20]. Ionic protein-lipid interactions depend on the proximity between lipid and protein molecules. In a previous study, we find that increasing the distance between juxtamembrane polybasic region with the membrane by inserting a

flexible linker after transmembrane domain can lead to the disruption of ionic protein-lipid interaction[33]. Such a strategy was applied there to disrupt $CD28_{CD}$-lipid interaction. A 10a.a. flexible linker (SSGSGPGSPS) was added in between CD28 transmembrane and cytoplasmic domain. This design preserves the native CD28 sequence for signaling but increases the distance between the CD28 basic residues and acidic phospholipids to reduce ionic interactions. To study the membrane binding of CD28 WT and linker mutant in live T cells, we applied the FRET strategy as the previous report[20]. We expressed a full-length CD28 WT or mutant construct with a C-terminal mTFP tag in Jurkat T cells whose membrane was labeled with the rhodamine dye R18. In this way, we expect the membrane-bound $CD28_{CD}$ to generate a stronger FRET intensity compared to the solvent-exposed $CD28_{CD}$. **Supplementary Fig. 6a** shows that the CD28 linker mutant had significantly reduced membrane binding in live T cells. We transduced CD28 WT or the linker mutant into $CD28^{-/-}$ mouse cytotoxic T cells. Since these cells were pre-activated, we observed basal phosphorylation and signaling of CD28 WT. It was evident that CD28 linker mutant had more basal phosphorylation and more associations with p85, Lck and Grab2 (**Supplementary Figs. 6b,c**). One of the major co-stimulation functions of CD28 is the enhancement of IL-2 production induced by TCR. We therefore measured IL-2 production to test whether changing CD28-membrane binding could directly impact its co-stimulation function. Direct comparison in resting T cells was not possible because IL-2 production was too low. We then used α-CD3 alone to stimulate T cells, and observed significantly more IL-2 from T cells with CD28 linker mutant. When α-CD28 was supplied together with α-CD3 to fully activate both CD28 WT and linker mutant, the production of IL-2 from both cells were comparable (**Supplementary Figs. 6d,e**). Collectively, these data support the notion that the membrane binding of $CD28_{CD}$ limits its basal signaling in T cells.

TCR signaling leads to the increase of local Ca^{2+} concentration around CD28

Our previous work has shown that TCR signaling leads to a local increase in [Ca^{2+}] and Ca^{2+} disrupts ionic CD3-lipid interactions by direct binding to the negatively-charged phosphate groups of acidic phospholipids[24]. The binding to phospholipid phosphate group is specific to Ca^{2+} but not Mg^{2+} and Zn^{2+} [34]. Upon T cell activation, CD28 is initially co-localized with TCR in peripheral microclusters that move towards the center of the immune synapse[35]. We therefore hypothesized that TCR-induced local [Ca^{2+}] increases can also affect ionic CD28-lipid interaction.

We firstly fused GCaMP6f, an ultrasensitive and fast Ca^{2+} indicator[36], to the tail of CD28 to monitor local Ca^{2+} concentration (**Fig. 3**). Anti-CD3 alone induced dramatic CD28-GCaMP6f signal increase in both the antibody-induced immunological synapse and the peripheral region. Anti-CD28 alone was not able to induce such a change. Thus, CD28-GCaMP6f signal increase was specifically caused by TCR-induced Ca^{2+} influx but not CD28 pooling. In the context of α-CD3 stimulation, α-CD28 can

further enhance the CD28-GCaMP6f signal, which echoes earlier finding showing that CD28 signaling augments TCR-induced Ca^{2+} influx[37]. We noticed the presence of hot spots with strong CD28-GCaMP6f signals that were > 60 fold higher than the basal signal, suggesting the formation of local Ca^{2+} microdomains with high [Ca^{2+}] surrounding CD28. When Ca^{2+} was not present in the stimulating buffer, CD28-GCaMP6f signal increase was not observed, supporting the notion that Ca^{2+} ions influxed from outside but not those released from intracellular ER stores contributed to the local Ca^{2+} enrichment around CD28. Earlier studies also found that Ca^{2+} release from ER store played a minor role in intracellular [Ca^{2+}] increase in T cells[38]. Ca^{2+} microdomain is a common structure found in many cell types, which is caused by fast influx of Ca^{2+} ions via open Ca^{2+} channels that can not be immediately buffered by cytosol[39]. The estimated [Ca^{2+}] in the Ca^{2+} microdomain is tens-hundreds micromole.

All together, the Ca^{2+} imaging results show that TCR signaling induces local enrichment of Ca^{2+} ions around CD28.

Ca^{2+} induces the open conformation of CD28 cytoplasmic domain to facilitate CD28 signaling

We firstly performed the microdialysis assay to show that the increase of [Ca^{2+}] resulted in substantial reduction of the binding of $CD28_{CD}$ with acidic phospholipids (**Fig. 4a**). This disruption effect of Ca^{2+} was also confirmed by NMR measurements. In response to the increase of [Ca^{2+}] concentration, $CD28_{CD}$ amide resonances exhibited systematic shifts from the membrane-bound state to the solvent-exposed state (**Fig. 4b**). Moreover, adding Ca^{2+} substantially weakened the tyrosine–lipid NOE signals in $CD28_{CD}$ + POPG bicelle sample (**Fig. 4c**), which indicated that the tyrosine sidechains were no longer fully inserted into the membrane interior. The AFE experiment also showed the dissociation of tyrosine sidechains from the membrane (**Figs. 4d,e**).

To test the effect of Ca^{2+} in live T cells, we applied the FRET strategy to monitor the membrane binding status of the $CD28_{CD}$. Two control constructs, 3aa-mTFP and 50aa-mTFP, were used to reflect the FRET efficiency of membrane-bound CD28 and membrane-dissociated CD28[25]. We found that Ca^{2+} influx induced by TCR stimulation or ionomycin treatment could disrupt the ionic CD28-lipid interaction and result in dissociation of $CD28_{CD}$ from the membrane (**Figs. 5a,b, Supplementary Fig. 7a**). In contrast, Ca^{2+} influx had no effect on the control 3aa and 50aa constructs because they did not have ionic protein-lipid interactions (**Supplementary Figs. 7b,c**). Stronger Ca^{2+} influx could cause higher degree of CD28 dissociation as shown by the α-CD3 titration experiment (**Supplementary Figs. 8a,b**). When the intracellular Ca^{2+} ions were partially chelated by BAPTA, the effect of Ca^{2+} on CD28-membrane binding was significantly impaired (**Supplementary Fig. 8a,b**). These experiments together show that Ca^{2+} can specifically disrupt CD28-lipid interaction in a

dose-dependent manner. To determine whether the effect of Ca^{2+} relied on its charge property or signaling capacity, we replaced Ca^{2+} by Sr^{2+}, a non-physiological ion that preserves the charge property of Ca^{2+} but does not induce Ca^{2+}-dependent signaling in T cells[24]. Sr^{2+} influx, most likely via the Ca^{2+} channel-associated TRPC5 channel[40], also led to the dissociation of $CD28_{CD}$ from the membrane to similar extent as Ca^{2+} influx (**Figs. 5a,b**). It follows that the charge property of Ca^{2+} specifically modulates the ionic $CD28_{CD}$-lipid interaction.

In addition to Ca^{2+}, CD28 ligation also induced dissociation of $CD28_{CD}$ from the membrane and this effect was independent of Ca^{2+} (**Figs. 5c,d**) and CD28 signaling (**Supplementary Fig. 9a**), which suggest that receptor ligation might induce CD28 clustering and/or conformational change to dislodge $CD28_{CD}$ from the membrane. However, even in the context of CD28 ligation, the TCR-induced Ca^{2+} influx led to further membrane dissociation of $CD28_{CD}$ (**Figs. 5c,d**). It is worthy to note that CD28 ligands are largely unavailable under certain scenarios. Tumor cells often express low levels of CD28 ligands (**Supplementary Fig. 10**), and the upregulation of CTLA4 in tumor-infiltrating T cells also limits CD28 engagement with its ligands because CTLA4 has higher affinity to CD80/86[41]. Therefore, the role of Ca^{2+} in promoting CD28 opening can be more dominant in the tumor microenvironment.

Following membrane dissociation of $CD28_{CD}$, local tyrosine kinases and phosphatases regulate tyrosine phosphorylation of its signaling motifs. It was evident that TCR signaling was required for CD28 phosphorylation, because CD28 ligation alone did not lead to appreciable levels of phosphorylation (**Supplementary Fig. 9b**). We found that in primary T cells Ca^{2+} enhanced phosphorylation of CD28 and the recruitment of downstream signal proteins like p85, Lck and Grb2, in the presence of TCR ligation (**Fig. 5e**). Sr^{2+} can replace Ca^{2+} for enhancing CD28 signaling (**Fig. 5e**). Chelating intracellular Ca^{2+} by BAPTA significantly impaired the enhancement effect of Ca^{2+} on CD28 signaling (**Supplementary Fig. 8c**). These functional experiments echo the FRET observations and they together show that Ca^{2+} can use its charge to enhance CD28 opening and signaling.

Integrated positive feedback between the TCR and CD28 mediated by Ca^{2+} can increase T cell antigen sensitivity

We next sought to formulate a mechanistic mathematical model that can explain the coupling between receptor phosphorylation, conformational change, and the interdependency of these observations with feedback through Ca^{2+} (**Fig. 6a**). The model includes both the TCR and CD28 that can exist in a closed, open, and phosphorylated open states when free or bound by ligand (see Methods details, including parameter values). When phosphorylated, the TCR is well known to lead to Ca^{2+} influx, and similarly, phosphorylated CD28 can augment this TCR-induced Ca^{2+} influx by enhancing PLCγ1 phosphorylation[37]. The production of Ca^{2+} by these receptors increases their transition rates from the closed to the open state, as we have

shown experimentally here for CD28 and in a previous report for TCR[24], leading to positive feedbacks. The TCR-Ca^{2+} and CD28-Ca^{2+} feedbacks can be integrated through Ca^{2+} to form a dual-feedback circuit. Our mathematical model resembles the standard model for the different conformational states of G-protein Coupled Receptors[42].

This basic model was then used to determine the minimal set of assumptions necessary to explain our experimental findings, in the spirit of formulating minimal models of T cell activation[43,44]. Firstly, a second crosstalk mechanism, in addition to Ca^{2+} feedback, must exist between the TCR and CD28 to explain CD28 phosphorylation in the absence of Ca^{2+}. Stimulation with both α-CD3 and α-CD28 is necessary for phosphorylation of CD28 (**Supplementary Fig. 8b**), indicating that CD28 phosphorylation is TCR-dependent. Importantly, CD28 becomes phosphorylated even in the absence of Ca^{2+}, though to a much lower extent (**Fig. 5e**). We therefore allow phosphorylated TCR to phosphorylate open CD28, independently of Ca^{2+}, and the underlying mechanism may involve recruitment of Lck. Secondly, we included the ability of phosphorylated TCR to phosphorylate other open TCRs because phosphorylated TCR can induce the local activation of Lck[45]. Since the efficiency of the reaction is determined by proximity and ligand binding induces proximity, we assume different rates for phosphorylation of free and bound TCR.

We find that with these assumptions, the model is able to reproduce the experimental observations (**Fig. 6b**). For example, the model recapitulates the observation that TCR ligation alone induces sufficient Ca^{2+} to promote the transition of CD28 from the closed to the open state (**Fig. 6b** (3rd column) for model and **Figs. 5a,b** for experiment). In addition, ligation of CD28 in the absence of ligands to the TCR (**Fig. 6b**, at low TCR ligand concentration) does not lead to CD28 phosphorylation but CD28 opening (experimental data shown in **Figs. 5c,d, Supplementary Fig. 9b**).

The model highlights that TCR phosphorylation is increasingly more sensitive to the TCR ligand dose in the presence of Ca^{2+} feedback (**Fig. 6b**). CD28 co-stimulation can further increase the sensitivity. In fact, the model makes the prediction that TCR phosphorylation, CD28 phosphorylation and Ca^{2+} signal all exhibit a switch-like response at some threshold TCR ligand dose when Ca^{2+} and CD28 ligand are both present. The modeling data thus support the notion that the TCR-Ca^{2+}-CD28 circuit mediated by Ca^{2+} could contribute to the high antigen sensitivity of T cells.

DISCUSSION

Using a comprehensive set of methods, we have shown that electric charges carried by acidic phospholipids and Ca^{2+} ions play central roles in regulating CD28 signaling.

Acidic phospholipids distribute asymmetrically in the plasma membrane. They are

exclusively enriched in the inner-leaflet of the plasma membrane and tend to form nanoclusters to regulate local events[23,46]. In T cells, acidic phospholipids can ionically interact with the polybasic regions in CD3ε/ζ cytoplasmic domains, thus sequestering the ITAM motifs within the membrane to prevent spontaneous TCR activation[24,25,27-31]. CD28 cytoplasmic domain also contains evolutionarily conserved polybasic regions and our biochemical and live-cell imaging experiments have revealed that $CD28_{CD}$ interacts with acidic phospholipids in resting T cells. NMR structure shows that $CD28_{CD}$ is fully embedded into the lipid bilayer, with the key signaling sites sequestered in the membrane hydrophobic interior, which renders them inaccessible to downstream signaling molecules. Functionally, membrane binding indeed limits CD28 basal signaling in primary T cells (**Supplementary Fig. 6**). Intriguingly, the insertion levels of two tyrosine motifs in the membrane are different. The backbones of YxxM give stronger NOEs to lipid acyl chains than those of PYAP (**Figs. 1c,d**). Furthermore, the Tyr14 sidechain in the YxxM motif also shows stronger NOEs to lipid acyl chains than the Tyr32 sidechain in the PYAP motif (**Fig. 1f**). Therefore, both backbones and sidechains of the YxxM motif are inserted more deeply into the membrane compared with those of the PYAP motif. The Ca^{2+} titration experiment further confirms this tilted orientation of $CD28_{CD}$ within the membrane. The fact that, at the same Ca^{2+} concentration, the Tyr-to-lipid NOE signals from Tyr32 nearly diminish while those of Tyr14 are weaken but still preserved (**Fig. 4c**), suggests that the YxxM motif should be located at the deeper position in the membrane and therefore was more difficult to be released from the membrane. Upon T cell activation, different CD28 motifs might become open and functional in a temporal order.

Why CD28 signaling is largely dependent on TCR signaling is a longstanding question[21,22]. It is already known that human primary T cells require the colocalization of TCR and CD28 ligands for efficient IL-2 production[47]. Here we show that TCR-induced local [Ca^{2+}] increases can disrupt the CD28-lipid interaction and therefore enhance CD28 signaling. Also, active Lck is important for TCR-CD28 crosstalk[47]. Upon T cell activation, ligation of CD28 with CD80/86 results in the initial recruitment of CD28 into peripheral microclusters (MC) together with TCR, followed by the migration of CD28 into the immunological synapse where CD28 and TCR reside in neighboring subregions[35]. It should be noted that active Lck and Ca^{2+} microdomains are colocalized with TCR[24,47]. The close proximity of CD28 and TCR makes it possible for Ca^{2+} and active Lck to modify CD28 signaling. We indeed observed a good co-localization of Ca^{2+} microdomains with CD28 molecules by high-resolution real-time imaging (**Fig. 3)**. Ca^{2+} can stabilize $CD28_{CD}$ in the membrane-dissociated conformation, allowing the recruitment of Lck to the juxtamembrane polybasic region to mediate tyrosine phosphorylations and the recruitment of downstream molecules. When the density of native CD28 ligands is low, such as the case of tumor microenvironment (**Supplementary Fig. 10**), Ca^{2+}-mediated opening of $CD28_{CD}$ may become even more important in regulating CD28 signaling.

CD28 ligation alone can also selectively increase the transcription of a few genes including Bcl-xL, and IL-8[48-52]. This autonomous signaling relies on the recruitment of Vav-1, filamin-A and Grb2/Gad to activate IKKα and NIK[50,51,53,54]. **Figure 5d** shows that CD28 ligation indeed can cause the dissociation of the cytoplasmic domain from the membrane, although to a less extent compared with both TCR and CD28 ligations, which could be sufficient to turn on the autonomous signaling.

Another longstanding open question in T cell biology is how a single antigenic ligand can trigger the full effector function of T cells[55-58]. Positive feedback is a mechanism that can increase the sensitivity of cells to their stimuli. We have identified a positive feedback circuit among TCR, CD28, and Ca^{2+}. Mathematical modeling of this dual-feedback circuit has shown that it can increase the sensitivity of T cells to antigens more efficiently than individual feedback circuits (**Fig. 6**). Together with other feedback regulations[59,60], this circuit can provide a signaling basis for the high sensitivity of T cells to antigen. Previous works highlight the importance of kinases and phosphatases in regulating TCR and CD28 activation. Abundant phosphatases with high constitutive catalytic activity, such as CD45, keep receptors in a dephosphorylated state and that segregation of these phosphatases is necessary for signaling[61,62]. Here, we show that lipid-interaction can also contribute to restraining signaling and that the underlying mechanism is likely to be the inability of Lck to phosphorylate tyrosine-residues buried within the membrane. The molecular model we propose includes both of these phosphorylation-restraining mechanisms but in addition, includes critical positive feedbacks in receptor opening (via Calcium) and receptor phosphorylation necessary to overcome these restraints and initiate signaling. Another interesting point to mention is that Csk is found to be associated with phosphorylated CD28[17]. Given its inhibitory role on Lck activity[63], Csk might serve as a negative-feedback regulator to restrain CD28 phosphorylation.

In summary, we report a new mechanism regulating CD28 signaling, which involves a dynamic interplay between acidic phospholipids and Ca^{2+} that sets the local electrostatic environment. The ionic interactions of CD28-lipid and Ca^{2+}-lipid together regulate the accessibility of signaling motifs within CD28 to tyrosine kinases and phosphatases. The new mechanism provides new insights into two longstanding questions in T cell biology, namely, why CD28 signaling is mostly dependent on TCR signaling and how T cells achieve high sensitivity to foreign antigen. This mechanism also explains how CD28 signaling is maintained at basal levels in resting T cells. Since that many other membrane proteins, including receptors, signaling molecules, and adhesion molecules, also contain juxtamembrane polybasic regions (**Supplementary Data Set 1**), the electrostatic regulation identified in the present study may be widely applicable.

Acknowledgements

The NMR and imaging works were performed at the National Center for Protein Science Shanghai, and Core Facility for Molecular Biology of SIBCB, and Core Facility for Cell Biology of SIBCB. We thank Dr. Zhijun Liu of the NMR section, NCPSS, for the help of setting up filter NOESY experiments. We thank Yang Yu of the Integrated Laser Microscopy section, NCPSS, for the help of setting up imaging experiments. We thank Kai Wucherpfennig and Etienne Gagnon for the discussion at the early stage of this project. C.X. is funded by NSFC grants (No. 31370860, No. 31425009, No. 31530022, and No. 31621003), and CAS grants (Strategic Priority Research Program No. XDB08020100). H.L. is funded by NSFC grant (No. 31470734 and 31670751) and MOST No. 2014CB541903. O.D. is funded by a Sir Henry Dale Fellowship, jointly funded by the Wellcome Trust and the Royal Society (Grant Number: 098363). N.T acknowledges support from the Systems Biology DTC supported by the Engineering and Physical Science Research Council (UK).

Author contributions

C.X. conceived the project and wrote the manuscript. C.X., H.L., O.D. and H.S. designed the experiments. W.P. and H.L. performed the NMR experiments. W.Y., W.P. and S.J. performed the biochemical and immunological experiments. S.C. and W.Y. performed the imaging experiments. N.T. and O.D. performed the mathematical modeling. F.X., W.W. and S.C. performed the bioinformatics analysis. H.W., X.L. and H.J. provided extensive discussion. Z.P., M.X. helped the protein purification. X.L. and H.J generated BBN-14 cells. All authors contributed to the manuscript revision.

COMPETING FINANCIAL INTERESTS

The authors declare no competing financial interests.

References

1. Esensten, J.H., Helou, Y.A., Chopra, G., Weiss, A. & Bluestone, J.A. CD28 Costimulation: From Mechanism to Therapy. *Immunity* **44**, 973-88 (2016).
2. Chen, L. & Flies, D.B. Molecular mechanisms of T cell co-stimulation and co-inhibition. *Nat Rev Immunol* **13**, 227-42 (2013).
3. Rudd, C.E., Taylor, A. & Schneider, H. CD28 and CTLA-4 coreceptor expression and signal transduction. *Immunol Rev* **229**, 12-26 (2009).
4. Boomer, J.S. & Green, J.M. An enigmatic tail of CD28 signaling. *Cold Spring Harb Perspect Biol* **2**, a002436 (2010).
5. Salomon, B. et al. B7/CD28 costimulation is essential for the homeostasis of the CD4+CD25+ immunoregulatory T cells that control autoimmune diabetes. *Immunity* **12**, 431-40 (2000).
6. Tai, X., Cowan, M., Feigenbaum, L. & Singer, A. CD28 costimulation of developing thymocytes induces Foxp3 expression and regulatory T cell differentiation independently of interleukin 2. *Nat Immunol* **6**, 152-62 (2005).
7. Zhang, R., Borges, C.M., Fan, M.Y., Harris, J.E. & Turka, L.A. Requirement for CD28 in Effector Regulatory T Cell Differentiation, CCR6 Induction, and Skin Homing. *J Immunol* **195**, 4154-4161 (2015).
8. Linterman, M.A. et al. CD28 expression is required after T cell priming for helper T cell responses and protective immunity to infection. *Elife* **3**(2014).
9. Liang, Y. et al. The lymphoid lineage-specific actin-uncapping protein Rltpr is essential for costimulation via CD28 and the development of regulatory T cells. *Nat Immunol* **14**, 858-66 (2013).
10. Jain, N. et al. CD28 and ITK signals regulate autoreactive T cell trafficking. *Nat Med* **19**, 1632-7 (2013).
11. Martinez-Llordella, M. et al. CD28-inducible transcription factor DEC1 is required for efficient autoreactive CD4+ T cell response. *J Exp Med* **210**, 1603-19 (2013).
12. Diekmann, F. Immunosuppressive minimization with mTOR inhibitors and belatacept. *Transpl Int* **28**, 921-7 (2015).
13. Westhovens, R. et al. Clinical efficacy and safety of abatacept in methotrexate-naive patients with early rheumatoid arthritis and poor prognostic factors. *Ann Rheum Dis* **68**, 1870-7 (2009).
14. van der Stegen, S.J., Hamieh, M. & Sadelain, M. The pharmacology of second-generation chimeric antigen receptors. *Nat Rev Drug Discov* **14**, 499-509 (2015).
15. Kamphorst, A.O. et al. Rescue of exhausted CD8 T cells by PD-1-targeted

therapies is CD28-dependent. *Science* **355**, 1423-1427 (2017).
16. Hui, E. et al. T cell costimulatory receptor CD28 is a primary target for PD-1-mediated inhibition. *Science* **355**, 1428-1433 (2017).
17. Tian, R. et al. Combinatorial proteomic analysis of intercellular signaling applied to the CD28 T-cell costimulatory receptor. *Proc Natl Acad Sci U S A* **112**, E1594-603 (2015).
18. Dodson, L.F. et al. Targeted knock-in mice expressing mutations of CD28 reveal an essential pathway for costimulation. *Mol Cell Biol* **29**, 3710-21 (2009).
19. Kong, K.F. et al. A motif in the V3 domain of the kinase PKC-theta determines its localization in the immunological synapse and functions in T cells via association with CD28. *Nat Immunol* **12**, 1105-12 (2011).
20. Dobbins, J. et al. Binding of the cytoplasmic domain of CD28 to the plasma membrane inhibits Lck recruitment and signaling. *Sci Signal* **9**, ra75 (2016).
21. Diehn, M. et al. Genomic expression programs and the integration of the CD28 costimulatory signal in T cell activation. *Proc Natl Acad Sci U S A* **99**, 11796-801 (2002).
22. Riley, J.L. et al. Modulation of TCR-induced transcriptional profiles by ligation of CD28, ICOS, and CTLA-4 receptors. *Proc Natl Acad Sci U S A* **99**, 11790-5 (2002).
23. Li, L., Shi, X., Guo, X., Li, H. & Xu, C. Ionic protein-lipid interaction at the plasma membrane: what can the charge do? *Trends Biochem Sci* **39**, 130-40 (2014).
24. Shi, X. et al. Ca2+ regulates T-cell receptor activation by modulating the charge property of lipids. *Nature* **493**, 111-5 (2013).
25. Xu, C. et al. Regulation of T cell receptor activation by dynamic membrane binding of the CD3epsilon cytoplasmic tyrosine-based motif. *Cell* **135**, 702-13 (2008).
26. Zhang, H., Cordoba, S.P., Dushek, O. & van der Merwe, P.A. Basic residues in the T-cell receptor zeta cytoplasmic domain mediate membrane association and modulate signaling. *Proc Natl Acad Sci U S A* **108**, 19323-8 (2011).
27. DeFord-Watts, L.M. et al. The CD3 zeta subunit contains a phosphoinositide-binding motif that is required for the stable accumulation of TCR-CD3 complex at the immunological synapse. *J Immunol* **186**, 6839-47 (2011).
28. Deford-Watts, L.M. et al. The cytoplasmic tail of the T cell receptor CD3 epsilon subunit contains a phospholipid-binding motif that regulates T cell functions. *J Immunol* **183**, 1055-64 (2009).
29. Aivazian, D. & Stern, L.J. Phosphorylation of T cell receptor zeta is regulated by a lipid dependent folding transition. *Nat Struct Biol* **7**, 1023-6

583 (2000).
584 30. Gagnon, E., Schubert, D.A., Gordo, S., Chu, H.H. & Wucherpfennig, K.W. Local
585 changes in lipid environment of TCR microclusters regulate membrane
586 binding by the CD3epsilon cytoplasmic domain. *J Exp Med* **209**, 2423-39
587 (2012).
588 31. Bettini, M.L. et al. Membrane association of the CD3epsilon signaling
589 domain is required for optimal T cell development and function. *J Immunol*
590 **193**, 258-67 (2014).
591 32. Schwieters, C.D., Kuszewski, J.J., Tjandra, N. & Clore, G.M. The Xplor-NIH
592 NMR molecular structure determination package. *J Magn Reson* **160**, 65-73
593 (2003).
594 33. Chen, X. et al. Acidic phospholipids govern the enhanced activation of
595 IgG-B cell receptor. *Nat Commun* **6**, 8552 (2015).
596 34. Wang, Y.H. et al. Divalent cation-induced cluster formation by
597 polyphosphoinositides in model membranes. *J Am Chem Soc* **134**, 3387-95
598 (2012).
599 35. Yokosuka, T. et al. Spatiotemporal regulation of T cell costimulation by
600 TCR-CD28 microclusters and protein kinase C theta translocation.
601 *Immunity* **29**, 589-601 (2008).
602 36. Chen, T.W. et al. Ultrasensitive fluorescent proteins for imaging neuronal
603 activity. *Nature* **499**, 295-300 (2013).
604 37. Michel, F., Attal-Bonnefoy, G., Mangino, G., Mise-Omata, S. & Acuto, O. CD28
605 as a molecular amplifier extending TCR ligation and signaling capabilities.
606 *Immunity* **15**, 935-45 (2001).
607 38. Oh-Hora, M. et al. Dual functions for the endoplasmic reticulum calcium
608 sensors STIM1 and STIM2 in T cell activation and tolerance. *Nat Immunol*
609 **9**, 432-43 (2008).
610 39. Parekh, A.B. Ca2+ microdomains near plasma membrane Ca2+ channels:
611 impact on cell function. *J Physiol* **586**, 3043-54 (2008).
612 40. Ma, H.T. et al. Canonical transient receptor potential 5 channel in
613 conjunction with Orai1 and STIM1 allows Sr2+ entry, optimal influx of
614 Ca2+, and degranulation in a rat mast cell line. *J Immunol* **180**, 2233-9
615 (2008).
616 41. Collins, A.V. et al. The interaction properties of costimulatory molecules
617 revisited. *Immunity* **17**, 201-10 (2002).
618 42. Weiss, J.M., Morgan, P.H., Lutz, M.W. & Kenakin, T.P. The cubic ternary
619 complex receptor-occupancy model. III. resurrecting efficacy. *J Theor Biol*
620 **181**, 381-97 (1996).
621 43. Lever, M., Maini, P.K., van der Merwe, P.A. & Dushek, O. Phenotypic models
622 of T cell activation. *Nat Rev Immunol* **14**, 619-29 (2014).
623 44. Chakraborty, A.K. & Das, J. Pairing computation with experimentation: a
624 powerful coupling for understanding T cell signalling. *Nat Rev Immunol* **10**,

59-71 (2010).
45. Chakraborty, A.K. & Weiss, A. Insights into the initiation of TCR signaling. *Nat Immunol* **15**, 798-807 (2014).
46. van den Bogaart, G. et al. Membrane protein sequestering by ionic protein-lipid interactions. *Nature* **479**, 552-5 (2011).
47. Bashour, K.T. et al. Cross talk between CD3 and CD28 is spatially modulated by protein lateral mobility. *Mol Cell Biol* **34**, 955-64 (2014).
48. Marinari, B., Costanzo, A., Marzano, V., Piccolella, E. & Tuosto, L. CD28 delivers a unique signal leading to the selective recruitment of RelA and p52 NF-kappaB subunits on IL-8 and Bcl-xL gene promoters. *Proc Natl Acad Sci U S A* **101**, 6098-103 (2004).
49. Porciello, N. & Tuosto, L. CD28 costimulatory signals in T lymphocyte activation: Emerging functions beyond a qualitative and quantitative support to TCR signalling. *Cytokine Growth Factor Rev* **28**, 11-9 (2016).
50. Thaker, Y.R., Schneider, H. & Rudd, C.E. TCR and CD28 activate the transcription factor NF-kappaB in T-cells via distinct adaptor signaling complexes. *Immunol Lett* **163**, 113-9 (2015).
51. Takeda, K. et al. CD28 stimulation triggers NF-kappaB activation through the CARMA1-PKCtheta-Grb2/Gads axis. *Int Immunol* **20**, 1507-15 (2008).
52. Camperio, C. et al. CD28 ligation in the absence of TCR stimulation up-regulates IL-17A and pro-inflammatory cytokines in relapsing-remitting multiple sclerosis T lymphocytes. *Immunol Lett* **158**, 134-42 (2014).
53. Muscolini, M., Sajeva, A., Caristi, S. & Tuosto, L. A novel association between filamin A and NF-kappaB inducing kinase couples CD28 to inhibitor of NF-kappaB kinase alpha and NF-kappaB activation. *Immunol Lett* **136**, 203-12 (2011).
54. Piccolella, E. et al. Vav-1 and the IKK alpha subunit of I kappa B kinase functionally associate to induce NF-kappa B activation in response to CD28 engagement. *J Immunol* **170**, 2895-903 (2003).
55. Wertek, F. & Xu, C. Digital response in T cells: to be or not to be. *Cell Res* **24**, 265-6 (2014).
56. Huang, J. et al. A single peptide-major histocompatibility complex ligand triggers digital cytokine secretion in CD4(+) T cells. *Immunity* **39**, 846-57 (2013).
57. O'Donoghue, G.P., Pielak, R.M., Smoligovets, A.A., Lin, J.J. & Groves, J.T. Direct single molecule measurement of TCR triggering by agonist pMHC in living primary T cells. *Elife* **2**, e00778 (2013).
58. Davis, M.M. et al. T cells as a self-referential, sensory organ. *Annu Rev Immunol* **25**, 681-95 (2007).
59. Feinerman, O., Veiga, J., Dorfman, J.R., Germain, R.N. & Altan-Bonnet, G. Variability and robustness in T cell activation from regulated heterogeneity

in protein levels. *Science* **321**, 1081-4 (2008).
60. Das, J. et al. Digital Signaling and Hysteresis Characterize Ras Activation in Lymphoid Cells. *Cell* **136**, 337-351 (2009).
61. Cordoba, S.P. et al. The large ectodomains of CD45 and CD148 regulate their segregation from and inhibition of ligated T-cell receptor. *Blood* **121**, 4295-302 (2013).
62. James, J.R. & Vale, R.D. Biophysical mechanism of T-cell receptor triggering in a reconstituted system. *Nature* **487**, 64-9 (2012).
63. Tan, Y.X. et al. Inhibition of the kinase Csk in thymocytes reveals a requirement for actin remodeling in the initiation of full TCR signaling. *Nat Immunol* **15**, 186-94 (2014).

FIGURE LEGENDS

Figure 1. CD28 cytoplasmic domain inserts into the membrane bilayer

(A) Superimposed ^{1}H-^{15}N TROSY-HSQC spectra of $CD28_{CD}$ in phosphate buffer (red), in the presence of POPG bicelles (blue), and POPC bicelles (green).

(B) The ^{1}H-^{15}N TROSY-HSQC spectrum of ^{13}C, ^{15}N-labeled $CD28_{CD}$ in POPG bicelles with backbone assignments..

(C) Strips from ^{15}N-filtered NOESY spectrum of the same sample in (B), which show NOEs between backbone amide protons of $CD28_{CD}$ and methylene protons of lipid acyl chains, glycerol protons of lipid head groups (G1: 1st glycerol, G2: 2nd glycerol), and water protons.

(D) The bar graph representing the relative intermolecular NOE signals, i.e. the NOE signals between backbone amide protons of $CD28_{CD}$ and lipid acyl chains (green), lipid headgroups (red) and water molecules (blue). The lipid NOEs with Tyr14 and Met17 are not shown because of the signal overlapping. Percentages represent the relative intensities of NOE peaks normalized to the intensity of the diagonal peak.

(E) Selected strips showing methyl NOEs from a ^{13}C-methyl-filt-NOESY spectrum of $CD28_{CD}$ in POPG bicelles. Methyl-bearing side chains in leucines and methionines show strong NOEs to methylene protons of lipid acyl chain but only weak NOEs to lipid headgroup protons. The methyl group signals of Met15 and Met17 are overlapped.

(F) Strips from aromatic-filt-NOESY spectra of $CD28_{CD}$ wild type and two mutants (CD28_M4 and CD28_M5) in the context of POPG bicelles. These strips represent intermolecular NOEs between aromatic protons Hδ/Hε of tyrosines and methylene protons of lipid acyl chains. Some intramolecular NOEs of $CD28_{CD}$, such as the NOEs between aromatic protons of tyrosines and their neighboring Hα and Hβ protons, were detected because of incomplete isotope-filtering effects in NOESY experiments.

(G) Protein sequences of $CD28_{CD}$ WT and two mutants.

Figure 2. NMR structure of membrane-bound CD28 cytoplasmic domain

(A-C) The ribbon diagram of a representative structure from the side view (A) and the ensemble of 10 lowest-violation structures of $CD28_{CD}$ in POPG bicelles (B, C). Protein-lipid NOE signals were used to position $CD28_{CD}$ into the defined lipid planes that represent the lipid bilayer. The whole peptide is highly dynamic and has no

obvious secondary structure. $CD28_{CD}$ resides at the interface of the lipid acyl chain region and the headgroup region. The sidechains of the YxxM motif and the PYAP motif are shown, and the positions of the two PBRs (i.e. R5-R8 and R20-K27) are indicated. The right graph in panel A demonstrates the POPG structure. Panel C illustrates that the CD28 backbone has a narrow distribution at the vertical direction in the membrane bilayer. Moreover, the N-terminal part has a deeper position in the membrane than the C-terminal part.

(D-E) Side-by-side stereo views showing the sidechain orientations of the YxxM motif and the PYAP motif in the defined planes of the lipid bilayer (side view). Both tyrosine sidechains adopt the orientation toward the interior of the membrane.

(F-G) Side-by-side stereo views showing the basic residue orientations in the two PBRs (i.e. R5-R8 and R20-K27) in the defined planes of the lipid bilayer (side view). The sidechains of the basic residues adopt the orientations toward the membrane headgroups.

Figure 3. CD28-proximal Ca^{2+} concentration increases after TCR stimulation.

(A-D) The real time CD28-proximal Ca^{2+} images in the antibody-induced immunological synapse and in the peripheral region. GCaMP6f, an ultrasensitive and fast Ca^{2+} indicator, was fused to the C-terminus of mouse CD28. Plate-coated α-CD3 (5 μg/ml) and/or α-CD28 (5 μg/ml) antibodies were used to induce Ca^{2+} influx in T cells. TIRF microscopy and high-speed spinning-disc confocal microscopy were used to monitor CD28-promixal Ca^{2+} concentrations in the antibody-induced immunological synapse (A, B) and in the peripheral region (C, D). Mouse IgG was used as the isotype control antibody for α-CD3, and Syrian hamster IgG was used as the isotype control for α-CD28. A representative cell was selected from 16-30 cells in an image field and displayed for every condition. Panel B and D show the normalized Mean Fluorescence Intensity for whole immunological synapse or peripheral region at different time points. Bars in panel A and C represent 2 μm.

(E-H) Typical imaging pictures were selected from A and C at 60-second point to display the presence of CD28-proximal Ca^{2+} microdomains in both the antibody-induced immunological synapse and the peripheral region. Panel F and H show the normalized local Fluorescence Intensity along the line. Bars in panel E and G represent 2 μm.

Data are representatives of three independent experiments.

Figure 4. Ca^{2+} induces open conformation of $CD28_{CD}$

(A) The effect of Ca^{2+} in disrupting the ionic CD28-lipid interaction was measured by

the equilibrium-based microdialysis assay. Ca^{2+} was titrated into two chambers at a molar ratio of $[Ca^{2+}]$:[LUVs] from 0.02 to 1, i.e., with the Ca^{2+} concentration ranging from 0.1 to 5 mM.

(B) Superimposed ^{1}H-^{15}N TROSY-HSQC spectra of $CD28_{CD}$ with POPG bicelles (blue), $CD28_{CD}$ with POPG bicelles and Ca^{2+} with different concentrations (cyan, yellow and purple), and $CD28_{CD}$ with POPC bicelles (red). Ca^{2+} was titrated into the $CD28_{CD}$ + POPG bicelles sample at a molar ratio of $[Ca^{2+}]$/[POPG] from 0.2 to 0.8, i.e., with the Ca^{2+} concentration ranging from 1.5 to 6 mM.

(C) Strips are intercepted from ^{13}C-aromatic-filt-NOESY spectra of $CD28_{CD}$ WT, CD28_M4 and CD28_M5 in the context of POPG bicelles. NOEs between aromatic protons Hδ/Hε of tyrosines and methylene protons of lipid acyl chains were detected. Ca^{2+} was added to the sample to make $[Ca^{2+}]$/[POPG] = 0.2 ($[Ca^{2+}]$ = 1.5 mM)).

(D-E) The AFE assay was used to measure the effect of Ca^{2+} on the ionic $CD28_{CD}$-lipid interaction. Ca^{2+} was titrated in at a molar ratio relative to POPG of 0.05 to 0.3, i.e., with the Ca^{2+} concentration ranging from 10 to 60 μM.

Data are representatives of three (A and E) independent experiments, One-Way ANOVA was used to analyze difference among three groups, and unpaired *t*-test was used to analyze difference between two groups. The center value and error bar in **a** and **e** are detailed in Online Methods. Source data for **a**, **d** and **e** are available in Source Data 1.

Figure 5. TCR-induced Ca^{2+} influx enhanced $CD28_{CD}$ opening and signaling.

(A-B) The de-quenching FRET was used to detect the effect of TCR-induced Ca^{2+} influx on the $CD28_{CD}$-membrane interaction. Mouse CD28-mTFP expressing Jurkat cells were stimulated with α-CD3 (3 μg/ml) at 37 ^{o}C in Ca^{2+}/Mg^{2+}-free Ringer's buffer supplied with 1mM Ca^{2+}, 1mM Sr^{2+} or none, respectively. In (B), n = 47, 31, 31 (from left to right) for the three stimulation conditions. For the left and middle sub-panels, One-Way ANOVA was used to analyze difference among three groups (the p-values of left and middle sub-panels were <0.0001 and 0.00847) and unpaired *t*-test was used to analyze difference between two groups. For the right sub-panel, the mTFP level of the α-CD3 w/o Ca^{2+} group does not fit the normal distribution, Mann-Whitney test was used to compare this group with others.

(C-D) The de-quenching FRET was used to measure whether Ca^{2+} could further enhance the dissociation of $CD28_{CD}$ in the presence of CD28 crosslinking antibody. Mouse CD28-mTFP expressing Jurkat cells were stimulated with α-CD3 (3 μg/ml) plus α-CD28 (1 μg/ml) or α-CD28 alone at 37 ^{o}C in Ca^{2+}/Mg^{2+}-free Ringer's buffer supplied with 1 mM Ca^{2+} or none. Mouse IgG and Syrian hamseter IgG were used as the isotype controls of α-CD3 and α-CD28. In (D), n =36, 30, 33, 18 (from left to

right) for the four stimulation conditions. One-Way ANOVA was used to analyze difference among four groups, and the p-values were <0.0001, 0.6061 and 0.3642 from left to right. Unpaired *t*-test was used to analyze difference between two groups.

(E) The immunoprecipitation and immunoblotting assays were used to detect CD28 signaling. Mouse CTLs were stimulated with α-CD3 (0.5 μg/ml) plus α-CD28 (2 μg/ml) at 37 ^{o}C. The stimulating buffer (Ca^{2+}/Mg^{2+}-free Ringer's buffer) was supplied with 1 mM Ca^{2+}, 1 mM Sr^{2+} or none, respectively. The bands were quantitated by ImageJ. The pCD28/CD28, P85/CD28, Lck/CD28 and Grb2/CD28 ratios were obtained and further normalized to the value of no stimulation condition of each strip.

Data are representatives of three independent experiments. BP, before photobleaching, AP, after photobleaching. Bars in A and C represent 2 μm. In (B) and (D), each dot represents the FRET value from one individual cell. Original gel images of **e** can be found in **Supplementary Data Set 2**. Source data for **b** and **d** are available in Source Data 2.

Figure 6. Mathematical model of immune receptor conformational dynamics reveals the importance of Ca^{2+} feedback to the antigen sensitivity of T cells

(A) Schematic of the mathematical model showing that each receptor (TCR and CD28) can exist in an unphosphorylated closed (R_{closed}, C_{closed}), unphosphorylated open (R_{open}, C_{open}), and a phosphorylated open (R^{*}_{open}, C^{*}_{open}) state when free (R) or in complex with ligand (C).

(B) Computation of the model shows the fraction of TCR and CD28 in the closed (R_{closed} + C_{closed}), open (R_{open} + C_{open} + R^{*}_{open} + C^{*}_{open}), and phosphorylated (R^{*}_{open} + C^{*}_{open}) states with and without CD28 ligands or Ca^{2+}, as indicated.

The relative magnitude of the transition rates between receptor states are depicted by the size of the transition arrow. A detailed description of the model can be found in the Experimental Procedures.

Table 1. NMR and refinement statistics for membrane-bound $CD28_{CD}$

	Protein (PDB 2NAE)
NMR distance and dihedral constraints	
Distance constraints	
Total NOE	311
Intraresidue	103
Inter-residue	208
Sequential ($\|i - j\| = 1$)	79
Medium range ($2 \leq \|i - j\| \leq 4$)	10
Long range ($\|i - j\| \geq 5$)	0
Intermolecular	119
Hydrogen bonds	0
Total dihedral-angle restraints	0
ϕ	
ψ	
Structure statistics	
Violations (mean ± s.d.)	0
Distance constraints (Å)	
Dihedral-angle constraints (°)	
Max. dihedral-angle violation (°)	
Max. distance-constraint violation (Å)	
Deviations from idealized geometry	
Bond lengths (Å)	0
Bond angles (°)	0
Impropers (°)	
Average pairwise r.m.s. deviation (Å)[a]	
YxxM motif	
Heavy	0.26
Backbone	0.12
PYAP motif	
Heavy	0.62
Backbone	0.20

[a]Pairwise r.m.s.d. was calculated among 10 refined structures for the YxxM and PYAP motifs.

ONLINE METHODS

Reagents, cells and mice

Lipids and detergent (POPG, POPS, PI, PA, POPC and DHPC) were from Avanti polar lipids. Anti-human CD3ε (UCHT1) and anti-human CD28 (CD28.2) stimulating antibody were from eBioscience, anti-mouse CD3ε (145-2C11) and anti-mouse CD28 (37.51) stimulating antibodies and their corresponding secondary antibodies were from Biolegend except mentioned specifically. Anti-mouse IgG and anti-Syrian hamster IgG were also from Biolegend. For immunoprecipitation and immunoblotting, α-CD28 (M20) and α-Lck (3A5) were from Santa Cruz Biotechnology. α-pY100 (HRP conjugated), α-phospho-Akt (Thr308) (C31E5E) and α-Akt (pan) (C67E7) were from Cell Signaling Technology. α-P85 and α-Grb2 were from Abcam. For the flow cytometric analysis, PerCP-anti-mouse CD4, APC-anti-mouse IL-2 were from eBioscience, PE-anti-mouse CD80, PE-Cy7-anti-mouse CD86, and the corresponding isotype IgGs were from BD Biosciences. Isotopes for NMR experiments were from Cambridge Isotope Laboratories and Sigma.

CD28-deficient cell line was a generous gift from Oreste Acuto, Oxford University. CT26 murine colon carcinoma cell line and EL4 murine lymphoma cell line were from Cellbank of Chinese Academy of Sciences. Dendritic cells were differentiated from mouse bone marrow derived monocytes by culturing with GM-CSF and IL-4 for 4 days. The BNN-14 murine bladder carcinoma cell line derived from BBN (N-Butyl-N-(4-hydroxybutyl)nitrosoamine)-treated C57BL/6 mice and the *Eμ-Myc* $p19^{Afr-/-}$ mouse B cell lymphoma cell line derived from the *Eμ-Myc* transgenic mouse[64].

The CD28 knockout mice which were generated by Dr. Tak Mak from University of Toronto were from Jax Mice (#002666). All mice were maintained in pathogen-free facilities at the Institute of Biochemistry and Cell Biology. All animal experiments were approved by the Institutional Animal Care and Use Committee (IACUC) of Institute of Biochemistry and Cell Biology, Chinese Academy of Sciences.

Expression and purification of mouse CD28 cytoplasmic domain and mutants

The DNA fragment encoding mouse CD28 cytoplasmic domain ($CD28_{CD}$) or mutants was inserted into the pET-41a(+) vector (Novagen) and then transformed into *Escherichia coli* BL21 (DE3) cells. Cells were grown at 37 ^{o}C in M9 medium supplemented with one or more stable isotope labels until reaching an optical density at 600 nm of 0.6-0.8. After adding 0.2 mM IPTG, cells were further incubated at 37 ^{o}C for 6 h. Fusion protein was first purified by a GST affinity chromatography (Sigma), followed by tobacco etch virus (TEV) cleavage at 20 ^{o}C for 1 h to remove GST tag. Protein was further purified by reverse-phase HPLC using both semi-preparative and analytical C18 columns (Agilent) and was identified by MALDI-TOF mass spectrometry.

Equilibrium-based microdialysis assay

The microdialysis was performed as previously described[24,25]. The system contains an experimental chamber and a control chamber separated by a 300 kDa MWCO cellulose acetate membrane allowing for the movement of small peptide but not for the large unilamellar vesicles (LUVs). Both chambers contained 10 nM Alexa 488-labelled $CD28_{CD}$ and 5 mM LUVs in a microdialysis buffer containing 20 mM HEPES, pH 7.0 and 100 mM KCl. LUVs in the experimental chamber were made up of 100% of the acidic phospholipids POPG (PG), POPS (PS), PA, PI or a mixture designed to mimic the plasma membrane (40% POPC, 20% POPE, 20% POPS, 10% POPG, 10% PI), and LUVs in the control chamber were composed of 100% of the zwitterionic lipid POPC (PC). Ca^{2+} was titrated into two chambers at a molar ratio of [Ca^{2+}]:[LUVs] from 0 to 1. If $CD28_{CD}$ binds to acidic lipids but not zwitterionic lipids, the concentration of free $CD28_{CD}$ peptide in the experimental chamber would initially decrease because of the immobilization of $CD28_{CD}$ on the acidic phospholipid vesicles while the concentration of free $CD28_{CD}$ in the control chamber should remain constant. Lipid binding of $CD28_{CD}$ in the experimental but not the control chamber would lead to a free $CD28_{CD}$ concentration gradient across the chambers that would drive diffusion of $CD28_{CD}$ from the control chamber into the experimental chamber. At equilibrium (reached at 16 hours) we measured total fluorescence intensity of each chamber. The fluorescence intensity difference in the experimental chamber and the control chamber can reflect the binding efficiency of $CD28_{CD}$ to acidic phospholipids. The following equation was used for the calculation of lipid binding efficiency: Binding (%) = $(FL_{Exp} - FL_{Con})/(FL_{Exp} + FL_{Con})$ x 100. FL_{Exp} and FL_{Con} represent fluorescence intensity in the experimental chamber and the control chamber, respectively.

Aromatic fluorescence emission assay

$CD28_{CD}$ or Notch peptide and POPG bicelles (q = 0.8) were incubated at 37 ^{o}C for 5 min, and then detected on a Varian Cary Eclipse machine. The excitation wavelength was 275 nm and the emission scan was adjusted to cover the emission peak.

Bioinformatics analysis

SWISS-PROT was used as the source for human proteome database to screen for human proteins containing the keyword “Membrane” or without any description in the “Subcelluar Location” lines. The selected dataset was then input to the transmembrane topology predictor Memsat-SVM[65] to predict all the transmembrane proteins, including their TM regions, TM topologies and signal peptides. Here we excluded the proteins with TM length less than 10 aa, which are potentially semi-transmembrane proteins that are not fully crossing the membrane.

Before calculating the pI value of the first 10 amino acid sequence of the cytoplasmic domain, we remove all signal peptide sequences based on SP predictions by

Memsat-SVM. For those proteins whose juxtamembrane region length was less than 10 aa, the pI value of that region was not calculated. The pI value was calculated by using the online tool at the website http://web.expasy.org/compute_pi/.

We checked the expression and localization of these proteins at the website http://www.hprd.org, and chose the membrane proteins that localized at the plasma membrane (keywords: plasma membrane or cell surface). The membrane proteins expressed in immune cells (keywords of immune cells: lymphocyte, thymocyte, B cell, Bone marrow, $CD4^+$ cell, $CD8^+$ cell, Dendritic cell, Granulocyte, Leukocyte, Macrophage, Monocyte, T Cell and Natural killer cell) were also identified. Then, we double checked the predicted results against the PubMed records and revised them if they were inconsistent. Finally, we generated the list of single-pass transmembrane proteins at the plasma membrane in immune cells that contain juxtamembrane polybasic regions (length of 10 aa) with pI value larger than 11.

Fluorescence resonance energy transfer (FRET) measurements and data analysis

To detect the interaction between $CD28_{CD}$ and plasma membrane by FRET, mouse CD28 contained a C-terminal TFP tag was exogenously expressed in Jurkat T cells. 1 x 10^6 cells were collected and resuspended in 1 ml Ca^{2+}/Mg^{2+}-free Ringer's buffer (155 mM NaCl, 4.5 mM KCl, 10 mM D-glucose, 10 mM HEPES, pH 7.4) supplied with 0 or 1 mM $CaCl_2$. Mg^{2+} was excluded in the FRET, Ca^{2+} imaging and western blot experiments because Mg^{2+} influx has also been reported in T cells and Mg^{2+} has signaling function[66]. Although Mg^{2+} has much less binding capability to acidic phospholipids compared with Ca^{2+} [34] so it should not directly affect $CD28_{CD}$-membrane binding, it was excluded anyhow to avoid any potential influence. After staining 300 μl aliquot of cells with 2 μM membrane-labeling dye R18, a FRET acceptor of TFP, on ice for 5 min, the cells were loaded onto the center of 35 mm glass-bottom dish (Shengyou Biotechnology) for 5 min at room temperature. Ionomycin (Sigma), α-CD3 (UCHT1) + secondary antibody (goat-α-mouse IgG), α-CD28 (37.51) + secondary antibody (rabbit α-Syrian hamster IgG), or both α-CD3 and α-CD28 with their secondary antibodies, were added into the dish and incubated for 5 min to stimulate the cells. Mouse IgG was used as the isotype control antibody for α-CD3, and Syrian hamster IgG was used as the isotype control for α-CD28. The secondary antibody was used at the same concentration as the primary antibody. Then the dish was put on a Leica TCS SP5 microscope for imaging. The de-quenching method was used to detect the FRET efficiency between TFP (donor) and R18 (receptor) as previously described[24,25]. TFP was excited with Argon 458 nm laser line and visualized using detection at 470-550 nm, R18 was excited with 561 nm laser line and visualized using detection at 570-650 nm. We first selected a frame and fully photobleached R18 signal of whole cells by the 561 nm laser set at 100% efficiency for 30-60 seconds. We then quickly measured the increase of TFP fluorescence signal after R18 photobleaching and converted it to FRET efficiency. FRET efficiency was calculated based on the formula: FRET efficiency = $(FL_{AP}-FL_{BP})/FL_{AP}$, FL_{AP} and

FL_{BP} represent TFP fluorescence after and before R18 photobleaching, respectively. Since the photobleaching time is short, we did not observe any obvious cell shape change and non-specific photobleaching of TFP. Three linker constructs, 3aa, 25aa and 50aa, that have different length of flexible linker between the transmembrane domain and TFP serve as controls [24,25]. These linkers do not bind to membrane so they have different distances between TFP and the membrane, thus yielding different FRET efficiencies.

For most FRET experiments, mouse CD28-TFP was expressed in Jurkat WT cells. We used α-mCD28 to stimulate the mCD28 construct and the endogenous human CD28 was not activated. For the FRET experiments of CD28 WT and linker mutant in **Supplementary Fig. 6a**, mouse CD28-TFP was expressed in CD28-deficient Jurkat T cells.

Ca^{2+} imaging

Mouse CD28-GCaMP6f was expressed in CD28-deficient Jurkat T cells.

Confocal Ca^{2+} imaging

8-well imaging chambers (Lab-Tek) were coated with antibodies in PBS buffer (pH 9.0) at 4 ^{o}C for 8 hours. 5 μg/ml antibody (α-CD3 (UCHT1) and/or α-CD28 (37.51)) was used as stimulating antibody. Mouse IgG was used as the isotype control antibody for α-CD3, and Syrian hamster IgG was used as the isotype control for α-CD28. Ca^{2+}/Mg^{2+}-free Ringer's buffer was used to wash away unbound antibody. Cells expressing mCD28-GCaMP6f were resuspended in Ca^{2+}/Mg^{2+}-free Ringer's buffer supplied with or without 1 mM Ca^{2+}. Cells were added to the antibody-coated chamber for TIRF or spinning-disc imaging on the ZEISS Cell Obsever SD. For the TIRF imaging, images of mCD28-GCaMP6f were acquired every 1 s. For the spinning-disc confocal imaging, we adjusted the Z position above the cell-coverglass contact interface to the equatorial focal plane of the cell, and acquired the images every 1 s. The following equation was used to normalize the fluorescence intensity of T cells against the background: Normalized FI = (FI – background)/background. The imaging data were analyzed by Imaris software (Bitplane) and Imaging Pro Plus (Media Cybernetics).

For the condition of with Ca^{2+}, 1 mM Ca^{2+} was present in the buffer to mimic the physiological concentration of extracellular Ca^{2+} [67].

Plate reader Ca^{2+} imaging

Cells were pre-treated with 10 μM BAPTA-AM (Life technology) or DMSO in Ca^{2+}/Mg^{2+}-free Ringer's buffer at 37 ^{o}C for 30 minutes. Cells were then washed with Ca^{2+}/Mg^{2+}-free Ringer's buffer, and resuspended with this buffer supplied with 1mM Ca^{2+}, and aliquoted into 96-well plate. The plate was inserted into a BioTek NEO plate reader with 37 ^{o}C environment. The basal GCaMP6f fluorescence in the first 10

minutes was used as the baseline. Stimulating antibody was added at the 10-minute time point and GCaMP6f fluorescence was recorded afterward to reflect intracellular Ca^{2+} concentration.

Measurement of CD28 signaling and co-stimulation function

CD28 signaling in wildtype mouse T cells

To detect CD28 signaling in primary mouse T cells, CTLs were generated by stimulating splenocytes from OT-I transgenic mice with 10 nM $OVA_{257-264}$ peptide and 10 ng/ml IL-2 for 2 days, followed by culturing for another 2 days in the presence of 10 ng/ml IL-2. The cells were harvested and washed with PBS twice, then were suspended with ice-cold Ca^{2+}/Mg^{2+}-free Ringer's buffer supplemented with additional 1 mM Ca^{2+} or Sr^{2+} or none. To chelate the intracellular Ca^{2+}, the cells were pretreated with 10 μM BAPTA-AM in Ca^{2+}/Mg^{2+}-free Ringer's buffer for 30 minutes at 37 ^{o}C before stimulation. The ice-cooled cells were aliquoted and stimulated with 0.5 μg/ml α-CD3 (145-2C11) + 0.5 μg/ml secondary antibody (rabbit α-hamster IgG, Sigma) plus 2 μg/ml α-CD28 (37.51, Syrian hamster IgG) + 2 μg/ml secondary antibody (goat-α-Syrian hamster IgG) for indicated times at 37 ^{o}C. Stimulation reactions were terminated by ice-cold PBS. The cells were spin down and lysed in an immunoprecipitation buffer (1% NP40, 50 mM Tris-HCl, pH7.4, 155 mM NaCl, 2 mM EDTA, 2 mM Na_3VO_4, 20 mM NaF, and complete protease inhibitor cocktail and phosphatase inhibitor cocktail (Selleck)) and then subjected to CD28 immunoprecipitation with α-CD28 antibody (37.51) and protein G-conjugated magnetic beads (Life technology). For the detection of CD28 signaling, the immunoprecipitation samples were separated by SDS-PAGE, transferred onto PVDF membrane (Millipore) and subjected to immunoblotting with α-pY100 (HRP conjugated, Cell Signaling Technology), α-p85 (Abcam), α-Grb2 (HRP conjugated, Abcam) and α-CD28 (M20, Santa Cruz), respectively.

Comparison of signaling and co-stimulation function of CD28 WT and CD28 linker mutant

$CD28^{-/-}$ T cells were isolated from the spleen of $CD28^{-/-}$ mice and stimulated for 2 days with plate-coated α-CD3 (145-2C11, 5 μg/ml). The activated $CD28^{-/-}$ T cells were infected twice by retrovirus carrying TFP-T2A-HA tagged CD28 WT or linker mutant construct. T2A is a self-cleaving peptide[68] so that TFP and HA-CD28 were separated in transduced T cells. The infected cells were cultured for another 2 days. To detect basal CD28 signaling, the cells (with > 50% transduction efficiency) were lysed and subjected to CD28 immunoprecipitation with α-HA antibody (3F10, Roche) and protein G-conjugated magnetic beads. To detect IL-2 production, the infected cells were stimulated with plate-coated α-CD3 (145-2C11, 0.5 μg/ml) alone or α-CD3 (0.5 μg/ml) + α-CD28 (37.51, 2 μg/ml) for 4 hours in the presence of 5 μg/ml Brefeldin A in normal 1640 medium. Intracellular staining and flow cytometry were used to detect IL-2 production. $CD4^{+}$ TFP^{+} cells were gated and analyzed for

IL-2 production. The flow cytometric data were collected by ACEA Novocyte 2060R, and FlowJo (VersionX.07 for mac) was used for flow cytometric analysis

NMR spectroscopy

All NMR spectra were acquired at 300 K on Bruker Avance 600 MHz and 900 MHz spectrometers. NMR data were processed using the program NMRPipe and analyzed by NMRView[69] and KUJIRA[70]. Resonance assignments were made using the standard NMR techniques. Structures were calculated using the program Xplor-NIH Version 2.32 software package.

Experimental setup

Resonance assignments were made using the standard NMR techniques. NMR spectra acquired for the resonance assignments were 2D ^{1}H-^{15}N HSQC, ^{1}H-^{13}C HSQC, 3D HNCA, HN(CO)CA, HNCO, HN(CA)CO, HNCACB, CBCA(CO)NH, HBHA(CO)NH, C(CCO)NH, HC(C)H-TOCSY, and (H)CCH-TOCSY. Protein NOEs were assigned using 3D ^{15}N-separated NOESY-HSQC (120 ms mixing time) and ^{13}C-separated NOESY-HSQC (150 ms mixing time). NOEs between protein and POPG bilayer were measured using the following three experiments: a 3D ^{13}C F1-filtered, ^{15}N F3-separated NOESY experiment (180 ms mixing time) to detect the NOEs between the peptide backbone amide protons and POPG protons, a 3D ^{13}C F3-separated and double-^{13}C-filtered NOESY experiments (180 ms mixing time) to detect the NOEs between the peptide methyl protons and POPG protons, and a 2D proton NOESY to detect the aromatic side chain protons to POPG protons. In 2D NOESY experiment (120 ms mixing time), for the indirect dimension, the proton signals from $CD28_{CD}$ were suppressed by double ^{13}C filtering, and only lipid methylene protons evolved; for the direct dimension, the aromatic protons were selected by aromatic ^{13}C separation. The sample dissolved in 90% H_2O/10% D_2O was used in all measurements except the ^{13}C-methyl-filt-NOESY and ^{13}C-aromatic-filt-NOESY experiments, in which the sample dissolved in 90% D_2O/10% H_2O was used to achieve better water suppression and to reduce the spin diffusion effect.

^{1}H-^{15}N TROSY-HSQC experiments of $CD28_{CD}$ in solution or in the presence of POPG bicelles or POPC bicelles were performed with 0.2 mM ^{15}N-labeled $CD28_{CD}$ in solution or with 40 mM POPG bicelles (q = 0.8) or POPC bicelles (q = 0.8) in 20 mM PB buffer (pH 6.7). Ca^{2+} titration experiments were done with 0.05 mM ^{15}N-labeled $CD28_{CD}$, 7.5 mM POPG bicelles (q = 0.8) in 20 mM Bis-Tris (pH 6.7). ^{15}N backbones relaxation measurements were performed with 0.2 mM ^{15}N-labeled $CD28_{CD}$, 40 mM POPG bicelles (q = 0.8) in 20 mM PB buffer (pH 6.7). ^{13}C-aromatic-filt-NOESY experiments were accomplished with 0.05 mM ^{15}N, ^{13}C-labeled $CD28_{CD}$, 7.5 mM POPG bicelles (q = 0.8) in 20 mM Bis-Tris buffer (pH 6.7). Backbone assignments, ^{15}N-filtered NOESY and ^{13}C-methyl-filt-NOESY experiments were operated with 0.5 mM, ^{13}C, ^{15}N-labeled $CD28_{CD}$, 100 mM POPG bicelles (q = 0.8) in 20 mM PB buffer

(pH 6.7).

NMR structure determination of membrane-bound $CD28_{CD}$

Structures were calculated using the program Xplor-NIH Version 2.32 software package. The intramolecular restraints for $CD28_{CD}$ were derived from 3D ^{15}N-separated NOESY-HSQC and ^{13}C-separated NOESY-HSQC, respectively. The intermolecular protein-lipid restraints were derived from three filtered NOESY experiments to detect (1) the NOEs between the peptide backbone amide protons and POPG protons, (2) the NOEs between the peptide methyl protons and POPG protons, and (3) the NOEs between the aromatic side chain protons to POPG protons. In order to position $CD28_{CD}$ into the lipid bilayer, three parallel planes corresponding to the position of the lipid POPG molecule were set: the first POPG headgroup glycerol, the second POPG headgroup glycerol, and the hydrophobic acyl chain. Then the protein-lipid NOEs are categorized into three groups accordingly. The protein NOE restraints were enforced by flat-well harmonic potential, with the force constant ramped from 5 to 30 kcal $mol^{-1}Å^{-2}$, while those between protein protons and lipid planes were enforced with flat-well harmonic potentials (±D), with the force constant ramped from 2 to 30 kcal $mol^{-1}Å^{-2}$. The value of D, defined as the size of the flat well in Å, was assigned based on the NOE intensity and the dynamic properties of phospholipid bilayer. An ensemble of 200 structures was calculated from 192 protein NOE-derived restraints and 119 protein-lipid restraints using high temperature simulated annealing (from 1000 to 200 K) of an extended $CD28_{CD}$ polypeptide, then 10 conformers with the lowest number of violations were selected to describe membrane-bound structure of $CD28_{CD}$ (Ramachandran statistics for residues N3-A40: 32% in the favored region and 28% in the allowed region). The programs MOLMOL and PyMOL (DeLano Scientific, Palo Alto, CA) were used for analyzing the calculated structures and preparing the drawings of the structures.

Mathematical modeling

The rule-based modeling software BioNetGen[71] was used to generate the ordinary-differential-equation reaction network (**Fig. 6a**), which was integrated by *ode15s* to the steady-state in Matlab (Mathworks, MA), as in previous models of TCR phosphorylation[72].

We assume identical parameter values for both the transition rates of the TCR and CD28 between the closed, open, and open phosphorylated states (**Supplementary Table 1**). In the absence of ligand, the majority of receptors are in the closed state and therefore the ratio of the forward to reverse transition between R_{closed} and R_{open} is taken to be 0.05. Opening of the receptor is facilitated by the addition of ligand, and we take the ratio of the transition rates between C_{closed} and C_{open} to be 5. For phosphorylation of the receptor, we take the ratio of the forward to the reverse reaction to be 0.05 both in the absence (R_{open} <-> $R_{open,phosph}$) and in the presence of ligand (C_{open} <-> $C_{open,phosph}$). The kinetic parameters that determine these ratios are

not known but are expected to be large because these reactions represent conformational transitions and phosphorylation/dephosphorylation reactions that ultimately allow T cells to respond within 6-7 seconds of antigen binding [73]. We have therefore used values that would be consistent with these fast timescales (**Supplementary Table 1**). We also include the ability of phosphorylated TCR to phosphorylate other open TCR and open CD28. Detailed description of the mathematical model can be found in Supplementary Methods.

Statistical analysis

Statistical analyses were performed using GraphPad Prism (GraphPad Software, Inc.) All sample sizes are large enough to ensure proper statistical analysis. Statistical methods were mentioned in the figure legends, and significance was determined as indicated in the figure legends. $P > 0.05$ was considered as no significant difference (marked as 'ns' in figures and figure legends); $P < 0.05$ was considered significant; $*P < 0.05$; $**P < 0.01$; $***P < 0.001$. For the sample size $n \leq 4$, One-Way ANOVA was used for comparing three or more groups, and unpaired *t*-test was used for comparing two groups. For n >10, the data distribution is first checked by using D'Agostino & Pearson omnibus normality test. If the data fit the normal distribution, One-Way ANOVA (for three or more groups) or unpaired *t*-test (for two groups) is used; if data do not fit the normal distribution, Mann-Whitney test is used. The replicates in **Figs. 5b, d**, and **Supplementary Figs. 4f, 6a, 6c, 6e, 7, 8b**, and **9a** were independent cell samples. The replicates in **Figs. 4a, e**, and **Supplementary Figs. 2e-g, 3c, and 4d** were independent protein samples. The center value and error bar in **Figs. 4e, 5b, 5d**, **Supplementary Figs. 3c, 4d, 4f, 6a, 6c, 6e, 7, 8b**, and **9a** denote mean and s.e.m., while those in **Fig. 4a** and **Supplementary Figs. 2e-g** denote mean and range.

A Life Sciences Reporting Summary (**Supplementary Data Set 3**) and a Flow Cytometry Reporting Summary (**Supplementary Data Set 4**) for this article are available online.

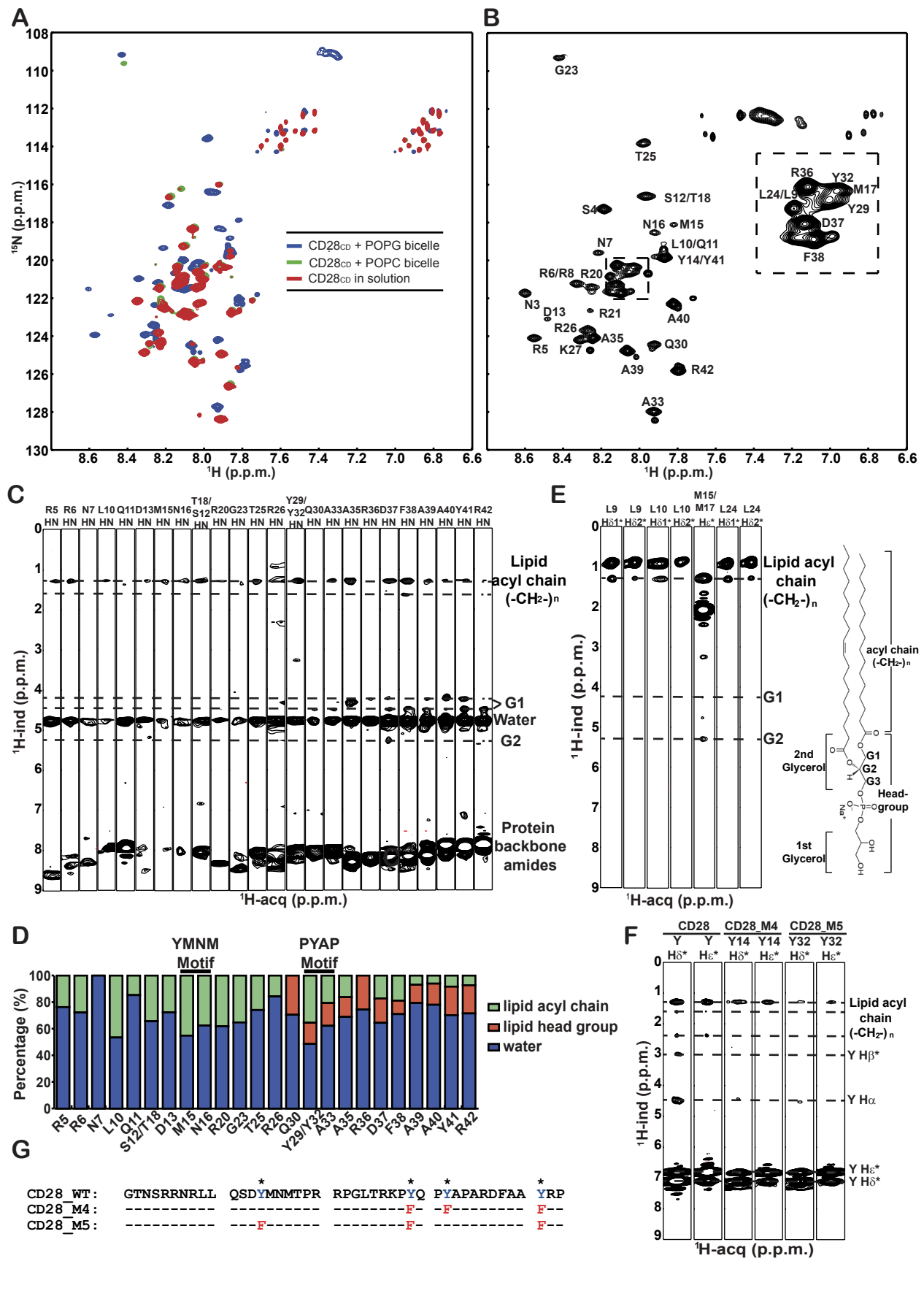
Data availability

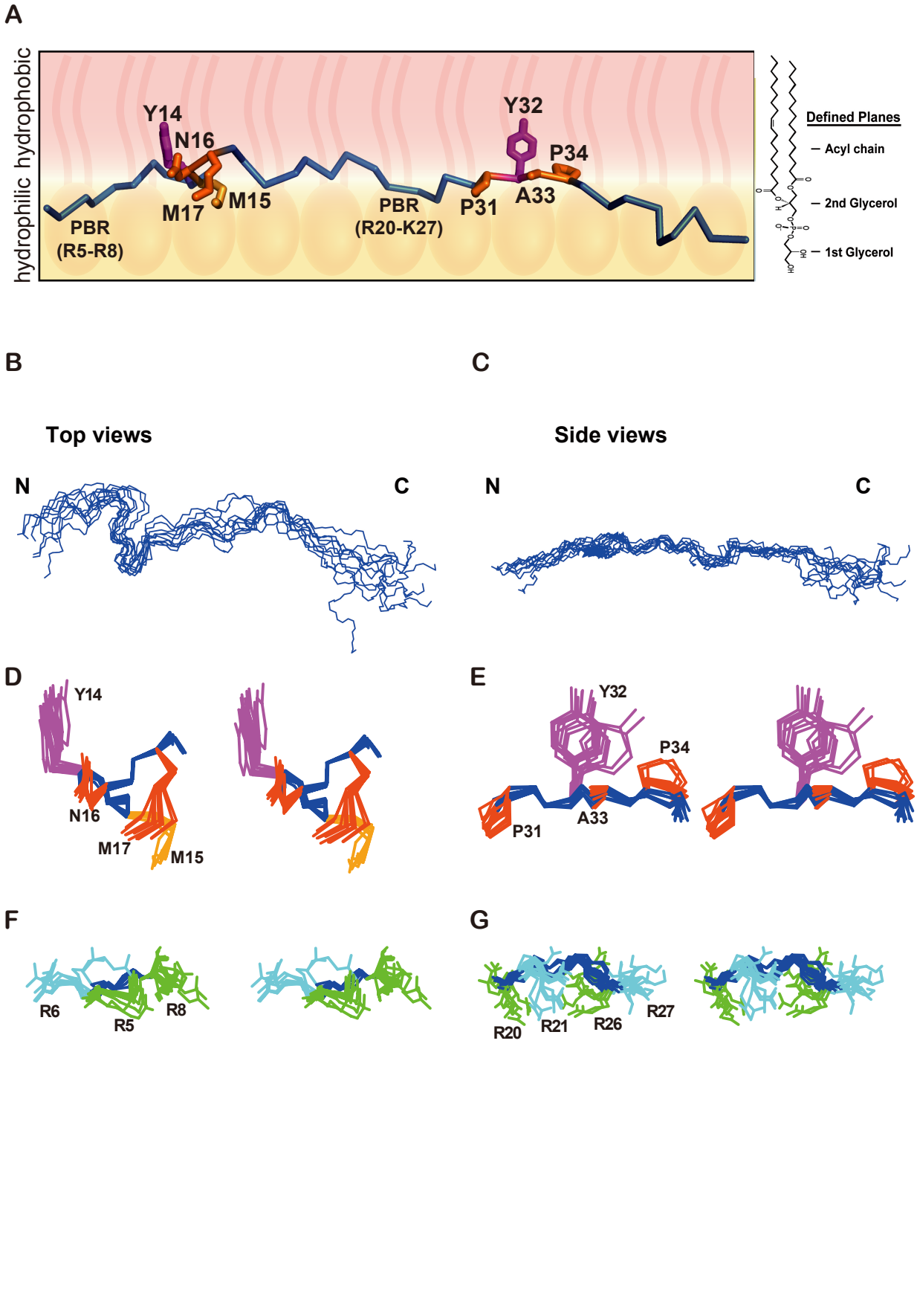
NMR coordinates have been deposited in the Protein Data Bank with PDB accession number 2nae and RCSB ID code rcsb104621. ^{1}H, ^{13}C, and ^{15}N chemical shifts have been deposited in the Biological Magnetic Resonance Bank with BMRB accession number 25935. Source data files for **Figs. 4a, 4e, 5b, 5d, Supplementary Figs. 1, 2e-g, 3c, 4d, 4f, 6a, 6c, 6e, 7, 8b, 9a** are available online. All other data are available from the corresponding authors upon reasonable request.

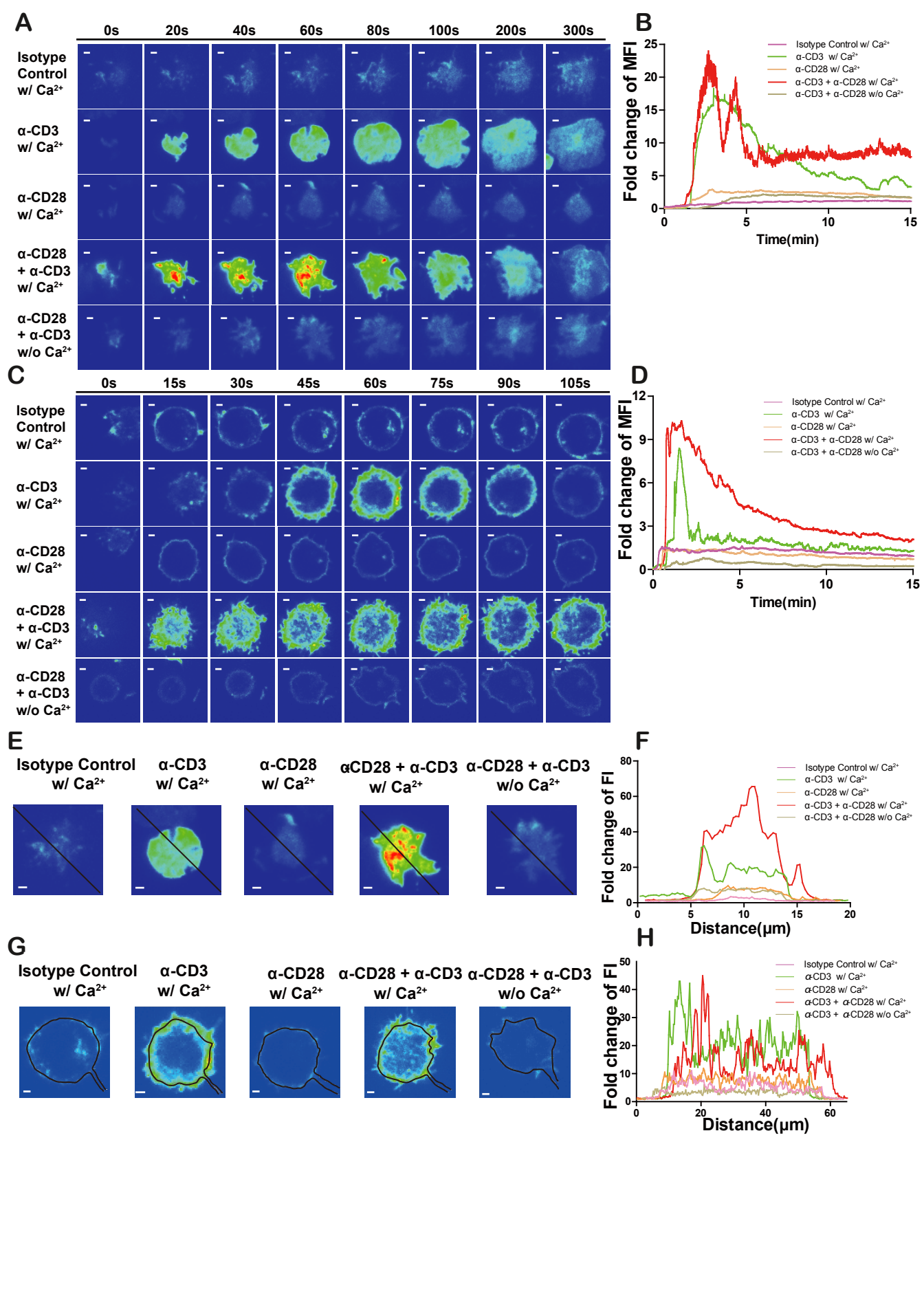
Methods of Jurkat cell activation and Definition of Mathematical Model are available in Supplementary Notes

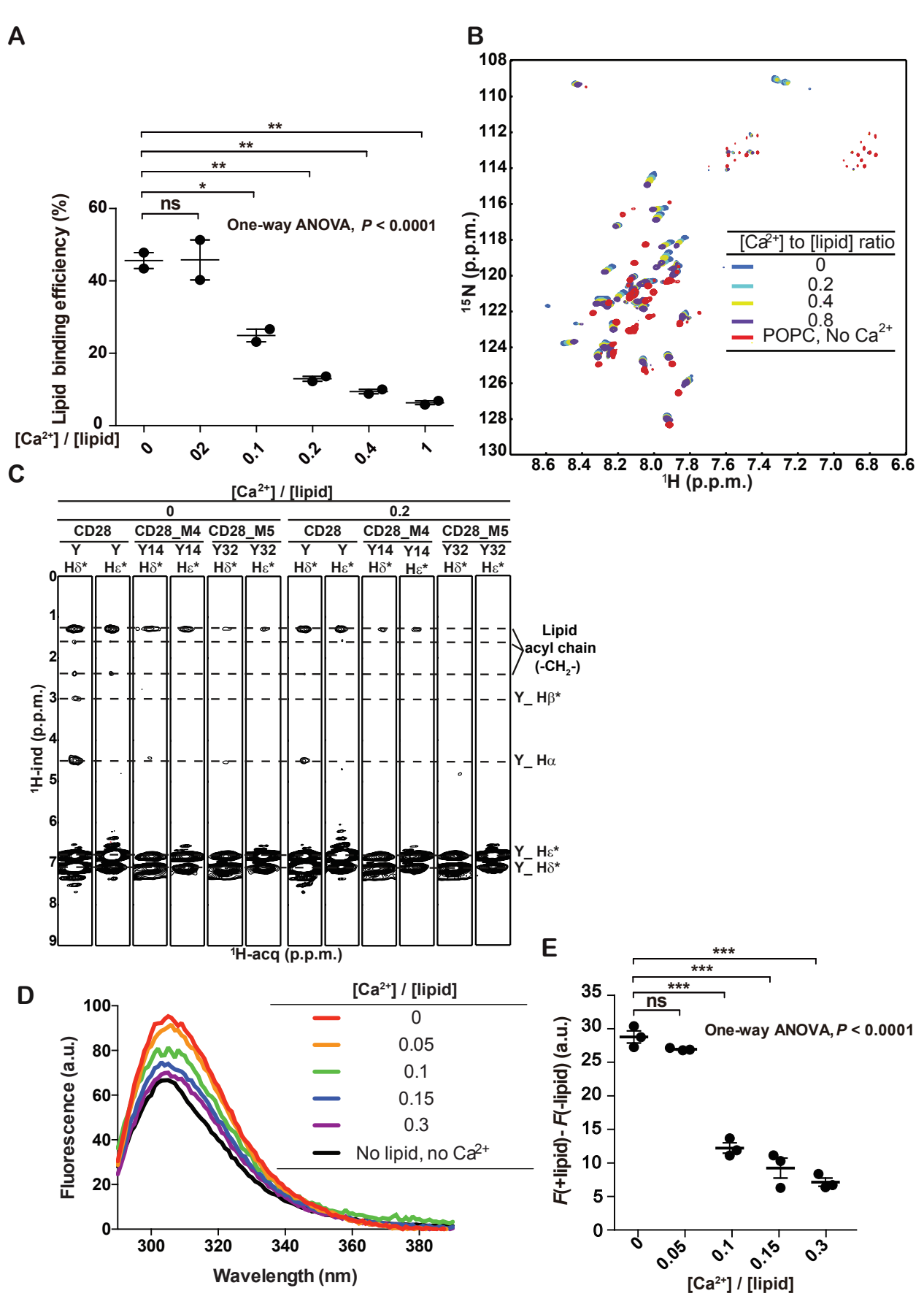
Methods-only References

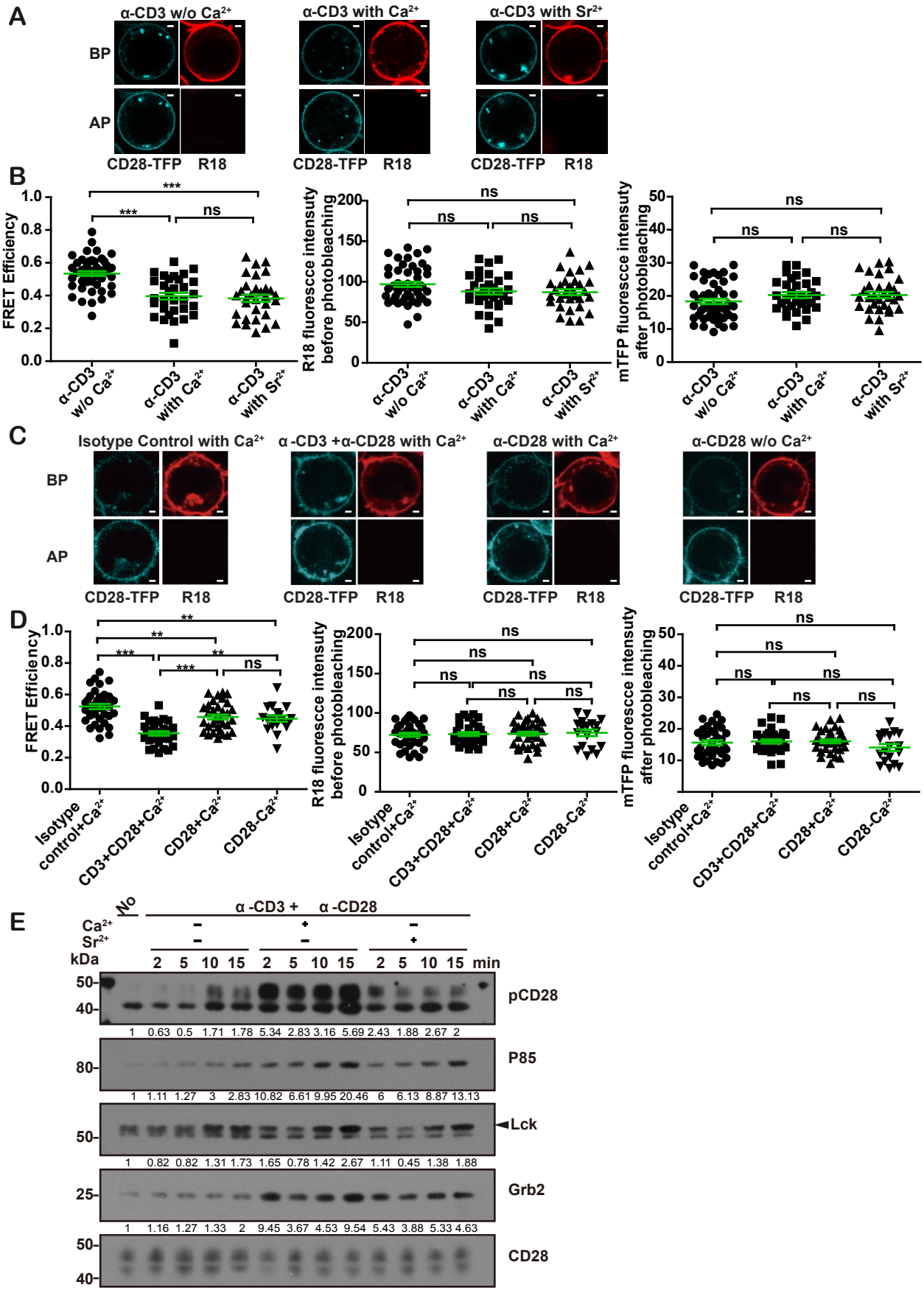
64. Schmitt, C.A., McCurrach, M.E., de Stanchina, E., Wallace-Brodeur, R.R. & Lowe, S.W. INK4a/ARF mutations accelerate lymphomagenesis and promote chemoresistance by disabling p53. *Genes Dev* **13**, 2670-7 (1999).
65. Nugent, T. & Jones, D.T. Transmembrane protein topology prediction using support vector machines. *BMC Bioinformatics* **10**, 159 (2009).
66. Li, F.Y. et al. Second messenger role for Mg2+ revealed by human T-cell immunodeficiency. *Nature* **475**, 471-6 (2011).
67. Hogan, P.G., Lewis, R.S. & Rao, A. Molecular basis of calcium signaling in lymphocytes: STIM and ORAI. *Annu Rev Immunol* **28**, 491-533 (2010).
68. Szymczak, A.L. et al. Correction of multi-gene deficiency in vivo using a single 'self-cleaving' 2A peptide-based retroviral vector. *Nat Biotechnol* **22**, 589-94 (2004).
69. Johnson, B.A. & Blevins, R.A. NMR View: A computer program for the visualization and analysis of NMR data. *J Biomol NMR* **4**, 603-14 (1994).
70. Kobayashi, N. et al. KUJIRA, a package of integrated modules for systematic and interactive analysis of NMR data directed to high-throughput NMR structure studies. *J Biomol NMR* **39**, 31-52 (2007).
71. Chylek, L.A. et al. Rule-based modeling: a computational approach for studying biomolecular site dynamics in cell signaling systems. *Wiley Interdiscip Rev Syst Biol Med* **6**, 13-36 (2014).
72. Mukhopadhyay, H., Cordoba, S.P., Maini, P.K., van der Merwe, P.A. & Dushek, O. Systems model of T cell receptor proximal signaling reveals emergent ultrasensitivity. *PLoS Comput Biol* **9**, e1003004 (2013).
73. Huse, M. et al. Spatial and temporal dynamics of T cell receptor signaling with a photoactivatable agonist. *Immunity* **27**, 76-88 (2007).

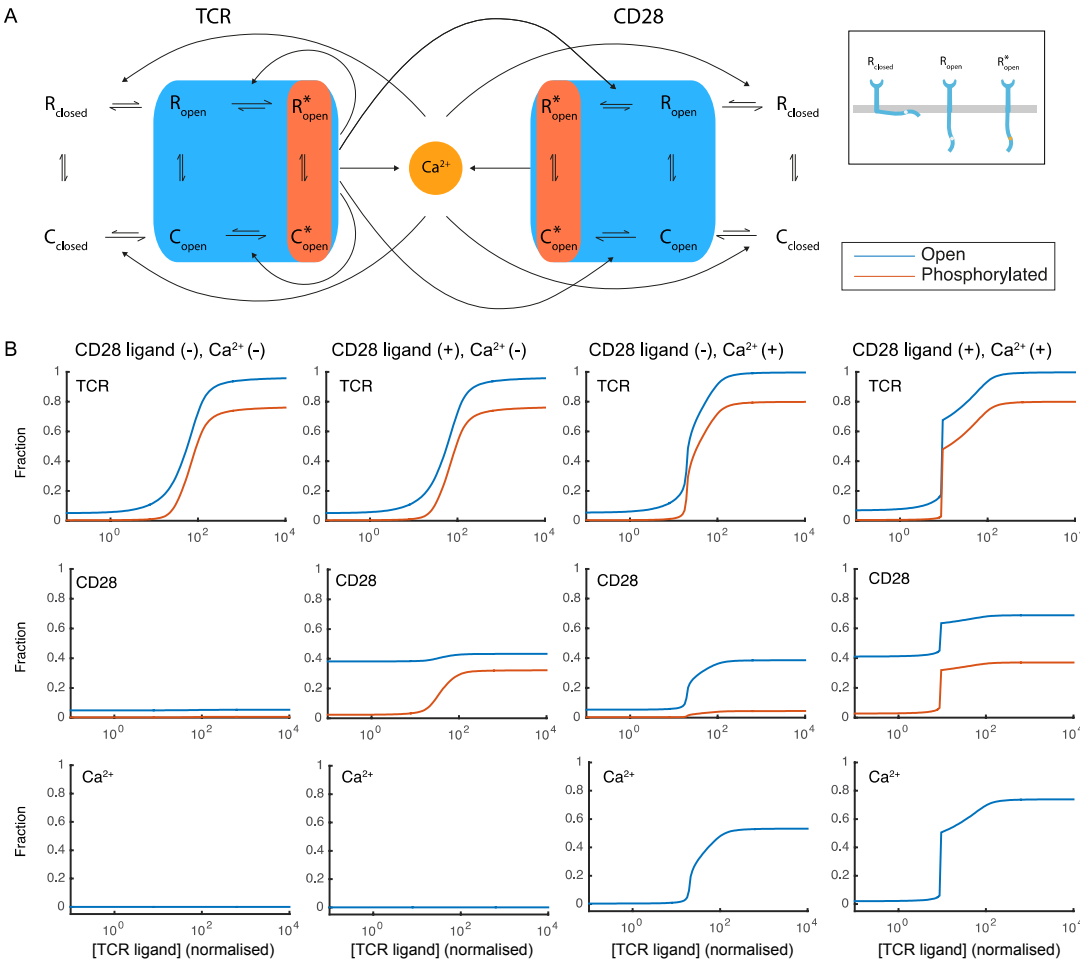

A
B
C
D
E
F
G
^{15}N (p.p.m.)
^{1}H (p.p.m.)
CD28CD + POPG bicelle
CD28CD + POPC bicelle
CD28CD in solution
G23
T25
S12/T18
S4
N16
M15
N7
L10/Q11
Y14/Y41
R6/R8
R20
N3
D13
R21
A40
R26
A35
R5
K27
Q30
A39
R42
A33
R36
Y32
M17
L24/L9
Y29
D37
F38
^{1}H-ind (p.p.m.)
^{1}H-acq (p.p.m.)
Lipid acyl chain (-CH2-)n
G1
Water
G2
Protein backbone amides
M15/ M17
acyl chain (-CH2-)n
2nd Glycerol
Head-group
1st Glycerol
YMNM Motif
PYAP Motif
Percentage (%)
lipid acyl chain
lipid head group
water
CD28
CD28_M4
CD28_M5
CD28_WT: GTNSRRNRLL QSDYMNMTPR RPGLTRKPYQ PYAPARDFAA YRP
CD28_M4: ---------- ---------- ---------F- -F--------- F--
CD28_M5: ---------- ---F------ ---------F- ---------- F--


A
hydrophilic hydrophobic
Y14
N16
M17
M15
PBR
(R5-R8)
PBR
(R20-K27)
P31
Y32
P34
A33
Defined Planes
Acyl chain
2nd Glycerol
1st Glycerol
B
Top views
N
C
C
Side views
N
C
D
Y14
N16
M17
M15
E
Y32
P34
P31
A33
F
R6
R5
R8
G
R20
R21
R26
R27


A
0s
20s
40s
60s
80s
100s
200s
300s
Isotype Control w/ Ca2+
α-CD3 w/ Ca2+
α-CD28 w/ Ca2+
α-CD28 + α-CD3 w/ Ca2+
α-CD28 + α-CD3 w/o Ca2+
B
Fold change of MFI
Time(min)
Isotype Control w/ Ca2+
α-CD3 w/ Ca2+
α-CD28 w/ Ca2+
α-CD3 + α-CD28 w/ Ca2+
α-CD3 + α-CD28 w/o Ca2+
C
0s
15s
30s
45s
60s
75s
90s
105s
Isotype Control w/ Ca2+
α-CD3 w/ Ca2+
α-CD28 w/ Ca2+
α-CD28 + α-CD3 w/ Ca2+
α-CD28 + α-CD3 w/o Ca2+
D
Fold change of MFI
Time(min)
Isotype Control w/ Ca2+
α-CD3 w/ Ca2+
α-CD28 w/ Ca2+
α-CD3 + α-CD28 w/ Ca2+
α-CD3 + α-CD28 w/o Ca2+
E
Isotype Control w/ Ca2+
α-CD3 w/ Ca2+
α-CD28 w/ Ca2+
αCD28 + α-CD3 w/ Ca2+
α-CD28 + α-CD3 w/o Ca2+
F
Fold change of FI
Distance(μm)
Isotype Control w/ Ca2+
α-CD3 w/ Ca2+
α-CD28 w/ Ca2+
α-CD3 + α-CD28 w/ Ca2+
α-CD3 + α-CD28 w/o Ca2+
G
Isotype Control w/ Ca2+
α-CD3 w/ Ca2+
α-CD28 w/ Ca2+
α-CD28 + α-CD3 w/ Ca2+
α-CD28 + α-CD3 w/o Ca2+
H
Fold change of FI
Distance(μm)
Isotype Control w/ Ca2+
α-CD3 w/ Ca2+
α-CD28 w/ Ca2+
α-CD3 + α-CD28 w/ Ca2+
α-CD3 + α-CD28 w/o Ca2+


A
Lipid binding efficiency (%)
[Ca2+] / [lipid]
0
02
0.1
0.2
0.4
1
ns
*
**
**
**
One-way ANOVA, P < 0.0001
B
15N (p.p.m.)
1H (p.p.m.)
[Ca2+] to [lipid] ratio
0
0.2
0.4
0.8
POPC, No Ca2+
C
[Ca2+] / [lipid]
0
0.2
CD28
CD28_M4
CD28_M5
Y Hδ*
Y Hε*
Y14 Hδ*
Y14 Hε*
Y32 Hδ*
Y32 Hε*
1H-ind (p.p.m.)
1H-acq (p.p.m.)
Lipid acyl chain (-CH2-)
Y_ Hβ*
Y_ Hα
Y_ Hε*
Y_ Hδ*
D
Fluorescence (a.u.)
Wavelength (nm)
[Ca2+] / [lipid]
0
0.05
0.1
0.15
0.3
No lipid, no Ca2+
E
F(+lipid)- F(-lipid) (a.u.)
[Ca2+] / [lipid]
ns
***
***
***
One-way ANOVA, P < 0.0001


A
α-CD3 w/o Ca2+
α-CD3 with Ca2+
α-CD3 with Sr2+
BP
AP
CD28-TFP
R18
B
FRET Efficiency
R18 fluorescce intensuty before photobleaching
mTFP fluorescce intensuty after photobleaching
***
ns
α-CD3 w/o Ca2+
α-CD3 with Ca2+
α-CD3 with Sr2+
C
Isotype Control with Ca2+
α -CD3 +α-CD28 with Ca2+
α-CD28 with Ca2+
α-CD28 w/o Ca2+
D
**
Isotype control+Ca2+
CD3+CD28+Ca2+
CD28+Ca2+
CD28-Ca2+
E
No
α -CD3 +
α -CD28
Ca2+
Sr2+
kDa
2 5 10 15 2 5 10 15 2 5 10 15 min
50-
40-
pCD28
1 0.63 0.5 1.71 1.78 5.34 2.83 3.16 5.69 2.43 1.88 2.67 2
80-
P85
1 1.11 1.27 3 2.83 10.82 6.61 9.95 20.46 6 6.13 8.87 13.13
Lck
1 0.82 0.82 1.31 1.73 1.65 0.78 1.42 2.67 1.11 0.45 1.38 1.88
25-
Grb2
1 1.16 1.27 1.33 2 9.45 3.67 4.53 9.54 5.43 3.88 5.33 4.63
CD28


A
TCR
CD28
R closed
R open
R* open
C closed
C open
C* open
Ca2+
Open
Phosphorylated
B
CD28 ligand (-), Ca2+ (-)
CD28 ligand (+), Ca2+ (-)
CD28 ligand (-), Ca2+ (+)
CD28 ligand (+), Ca2+ (+)
TCR
CD28
Ca2+
Fraction
[TCR ligand] (normalised)